Effect of Disorder on Bulk Sound Wave Speed : A Multiscale Spectral Analysis.

Rohit Kumar Shrivastava[1] and Stefan Luding[1]

[1]Multiscale Mechanics (MSM), MESA+, Engineering Technology (ET), PO Box 217, 7500 AE Enschede, Netherlands

Correspondence to: Rohit Kumar Shrivastava(r.k.shrivastava@utwente.nl)

Abstract. Disorder of size (polydispersity) and mass of discrete elements/particles in randomly structured media (e.g. granular matter like soil) has numerous effects on the materials' sound propagation characteristics. The influence of disorder on energy and momentum transport, the sound wave speed and its low pass frequency filtering characteristics is the subject of this study. Goal is understanding the connection between the particle-micro-scale disorder and dynamics and the system-macro-scale wave propagation, which can be applied to non-destructive testing, seismic exploration of buried objects (oil, mineral, etc.) or to study the internal structure of the Earth. To isolate the longitudinal P-wave mode from shear and rotational modes, a one-dimensional system of equal size elements/particles is used to study the effect of mass disorder alone via (direct and/or ensemble averaged) real time signals, signals in Fourier space, energy and dispersion curves. Increase in mass disorder (where disorder has been defined such that it is independent of the shape of the probability distribution of masses) decreases the sound wave speed along a granular chain. Energies associated with the eigenmodes are conserved, independent of time, and can be used to obtain better quality dispersion relations for disordered chains; these dispersion relations confirm the decrease in pass-frequency and wave speed with increasing disorder acting opposite to the wave acceleration close to the source.

1 Introduction

Sound wave propagation through matter has been an extensive area of research (as textbook example, see Aki and Richards (2002)) whether it is applied for the study of earthquakes or the internal structure of the Earth, as well as oil, gas or mineral exploration (seismology). Waves can be used for dissecting the human body without using blades, revealing material properties through non-destructive testing (ultrasonics), studying the structure of lattices or designing metamaterials. There are numerous applications and uncountable problems which still need to be solved, where the challenge has always been resolving the finest structures of matter using wave propagation and hence, steps are being taken in the direction of micromechanics of seismic waves, see e.g. O'Donovan et al. (2016).

Disordered/Heterogeneous/Random media cause multiple scattering of seismic waves, mechanisms which eventually cause them to become dispersed, attenuated and localized in space (Sato (2011), Scales and Van Vleck (1997)). The phenomenon of multiple scattering causes the formation of the so called "coda" which is the tail of a propagating wave pulse. While coda was earlier treated as noise (Weaver (2005)), now it has given way to coda wave interferometry with multiple applications (Snieder et al. (2002)). The coda has been studied in detail in laboratory experiments with uniaxial or triaxial devices, for e.g., pulse

propagation across glass beads (Jia et al. (1999)), sintered glass beads (Güven (2016)), indicating extreme sensitivity towards system preparation and configuration and getting washed out on ensemble averaging with only the coherent part of the signal remaining. In Van Der Baan (2001), it was shown that macroscopic/seismic waves governed by the classical wave equation did not exhibit localization at lower frequencies but, this idea got repudiated by Larose et al. (2004), where weak localization (a mesoscopic phenomenon, precursor to wave localization; Sheng (2006)) was experimentally observed at frequencies as low as 20 Hz, indicating the inadequacy of the classical wave equation.

In recent years, wave propagation through granular materials has attracted a lot of attention. Granular material is a heterogeneous media with many discretized units and can be used for modeling geometrically heterogeneous media (Matsuyama and Katsuragi (2014)). The studies done using ordered/disordered lattices for wave propagation (Gilles and Coste (2003), Coste and Gilles (2008), etc.) has helped to understand wave propagation in granular materials through dispersion relations, frequency filtering, etc. Scaling laws allow to relate various physical parameters like density, pressure, coordination number, etc., with the moduli, forming an Effective Medium Theory (EMT) for granular matter (Makse et al. (2004)).

Nesterenko (1983) showed the existence of localized wave packets propagating in a non-linear granular chain (one dimensional granular material) under the condition of "sonic vacuum" (in the limit of zero acoustic wave speed and vanishing confining pressure) thus forming supersonic solitary waves; such concepts have been exploited immensely to develop various kinds of metamaterials like for shock and energy trapping (Daraio et al. (2006)), an acoustic diode (Boechler et al. (2011)) or for understanding and studying jamming transitions in granular matter (van den Wildenberg et al. (2013), Upadhyaya et al. (2014)). Some of the open questions and developments related to wave propagation in unconsolidated granular matter, like higher harmonics generation, non-linear multiple scattering, soft modes, rotational modes, etc., have been addressed by Tournat and Gusev (2010). However, in the following, the focus of attention will not be on solitons and unconsolidated granular matter, hence, there will be no occurrence of sonic vacuum during analyses (no opening and closing of contacts of particles).

A striking characteristic of consolidated granular matter is that grain-grain forces are arranged and correlated in a linear manner known as force chains (Somfai et al. (2005)). Similar to the force chains, Pasternak et al. (2015) showed the existence of moment chains in granular media, i.e. correlations of grain-grain mutual rotations. These chains are mesoscopic structures and are just one of the many micro-rotational effects of granules. Cosserat continuum theory can be used to model these micropolar/micro-rotational effects, as discussed in detail by Pasternak and Mühlhaus (2005).

The force chains/granular chains which carry the large forces of the system supposedly support faster sound transmission across granular matter (Ostojic et al. (2006)). In Owens and Daniels (2011), it was seen from experiments with 2-dimensional photo-elastic disks that vibration propagates along the granular chains, visualized by the brightness due to compression between the particles; however, the exact mechanisms of propagation of the vibrations are still a matter of ongoing research. Our system under investigation will be a single one of such granular chains (Fig. 1); it will assist in isolating the P-wave or the longitudinal excitation from all other kinds of excitations (S-wave, rotational wave, etc). In Merkel et al. (2010) it was seen that inclusion or removal of rotation does not significantly affect the longitudinal mode in an ordered granular crystal. However, the situation is different when rotations become prominent and other wave modes cannot be ignored (see Yang and Sutton (2015), Merkel and Luding (2016) and the references therein).
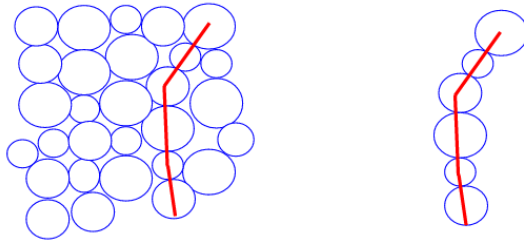
Figure 1. A granular/force chain from a network (schematic).

Even though very simplistic, a polydisperse granular chain can have two kinds of disorder, mass disorder and stiffness disorder (Lawney and Luding (2014)), the mass disorder has much stronger contribution towards disorder than stiffness because mass $\propto$ radius^3 whereas, stiffness $\propto$ radius$^{1/3}$ (Achilleos et al. (2016)). Hence, only mass disorder for the disordered granular chain has been chosen. However, there are processes when stiffness disorder cannot be ignored, for instance, the processes when the repulsive interaction force between the fragments/elements of the material being modeled has different stiffness during compression and tension (bilinear oscillator; Dyskin et al. (2014)), infinite stiffness while compression (impact oscillator; Dyskin et al. (2012) and Guzek et al. (2016)) or negative stiffness (Pasternak et al. (2014) and Esin et al. (2016)).

In Sect. 2 an impulse propagating across a granular chain is modeled. A similar model was used in Marketos and O'Sullivan (2013), Lawney and Luding (2014) and Otsubo et al. (2017). Section 2.8 concerns the dispersion relation for wave propagation across a granular medium, Sect. 2.9 concerns the group velocity and Sect. 2.10 concerns a novel way of computing the dispersion relation in terms of moments of eigenmodal energy. In Sect. 3, the quantities mentioned in Sect. 2 are computed and the observations are discussed. Sect. 4 summarizes and concludes the observations made in Sect. 3 with Sect. 2 as the foundation and an outlook of the ongoing as well as possible future research work on wave propagation in granular matter is given.

2 Modeling a general one-dimensional chain

A one-dimensional chain of $N+2$ particles is considered. Each particle i has mass $\tilde{m}^{(i)}$ and contact stiffness $\tilde{\kappa}_{(i,j)}$ with respect to a neighboring particle j. The tilde symbols are used for dimensional quantities. The interaction force experienced by neighboring particles i and j is

$$\tilde{F}_{(i,j)} = \tilde{\kappa}_{(i,j)}\tilde{\delta}_{(i,j)}^{1+\beta}, \qquad \tilde{\delta}_{(i,j)} \geq 0 \quad \text{and} \quad j = i \neq 1 \tag{1}$$

with the contact stiffness $\tilde{\kappa}_{(i,j)}$ and the particle overlap $\tilde{\delta}_{(i,j)} = \tilde{r}^{(i)} + \tilde{r}^{(j)} - |\tilde{x}^{(j)} - \tilde{x}^{(i)}|$, with the radius $\tilde{r}$ and co-ordinates $\tilde{x}$ of the centers of the particles. The Hertzian and linear model are given by $\beta = 1/2$ and $\beta = 0$, respectively (Lawney and Luding (2014)). This force acting from j on i is directed along $\hat{n} = -\frac{\tilde{x}^{(j)} - \tilde{x}^{(i)}}{|\tilde{x}^{(j)} - \tilde{x}^{(i)}|}$, corresponding in 1D to be positive and negative for $j < i$ and $j > i$, respectively. The force resembles the framework of the Discrete Element Method where the overlap of
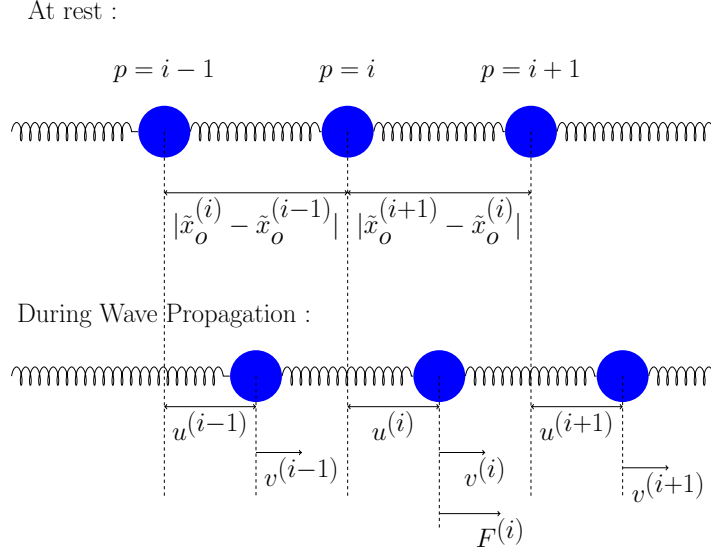
Figure 2. Pre-stressed chain of granular elements during dynamic wave propagation.

particles substitutes their deformations at the contacts, which would be much more difficult and time consuming to resolve with a finite element model of deformable bodies. Assume that the chain is pre-compressed by an external applied force $\tilde{F}_o$, the characteristic overlap of the particles in static equilibrium ($\tilde{\Delta}_o$) when all the contact stiffness ($\tilde{\kappa}_{(i,j)}$) of particles are chosen as $\tilde{\kappa}_o$ (characteristic contact stiffness) is thus defined as

$$\tilde{\Delta}_o = \left(\frac{\tilde{F}_o}{\tilde{\kappa}_o} \right)^{1/(1+\beta)}, \tag{2}$$

where the unit of $\tilde{\kappa}$ depends on β.

2.1 Non-dimensionalization

A length scale $\tilde{\ell}$ can be chosen such that the scaled particle overlap $\delta_{(i,j)} = \tilde{\delta}_{(i,j)}/\tilde{\ell}$ yields

$$\tilde{F}_{(i,j)} = \tilde{\kappa}_{(i,j)} \tilde{\ell}^{1+\beta} \delta_{(i,j)}^{1+\beta}. \tag{3}$$

There are several length scales $\tilde{\ell}$ that can be chosen, e.g. the particle size, the driving amplitude or the initial overlap

$$\Delta_{(i,j)} = \left(\frac{\tilde{F}_o}{\tilde{\kappa}_{(i,j)} \tilde{\ell}^{1+\beta}} \right)^{1/(1+\beta)} \tag{4}$$

of the particles in static equilibrium. The latter is chosen for computations here so that $\Delta_{(i,j)} = \Delta_o \equiv 1$ if all $\tilde{\kappa}_{(i,j)} = \tilde{\kappa}_o$. Other dimensionless quantities are, the mass $b = \tilde{m}/\tilde{M}_1$, where $\tilde{M}_1$ is the first moment of the mass distribution of the particles of the

media, as shown in Appendix C (the unscaled average mass of the particles), the dimensionless displacement $u = \tilde{u}/\tilde{l}$ and the dimensionless spring constant $\kappa = \tilde{\kappa}/\tilde{\kappa}_o$. The characteristic time scale becomes

$$\tilde{t}_c = \sqrt{\frac{\tilde{M}_1}{\tilde{\kappa}_o \tilde{\ell}^\beta}}, \tag{5}$$

which gives us the dimensionless time $t = \tilde{t}/\tilde{t}_c$. The displacement of particle i from its equilibrium position $\tilde{x}_o^{(i)}$ is $\tilde{u}^{(i)} = \tilde{\ell} u^{(i)} = \tilde{x}^{(i)} - \tilde{x}_o^{(i)}$, so that the overlap becomes, $\delta_{(i,j)} = \Delta_{(i,j)} - (u^{(j)} - u^{(i)})$. Finally, the interaction forces scales as

$$F_{(i,j)} = \frac{\tilde{t}_c^2}{\tilde{M}_1 \tilde{\ell}} F_{(i,j)}. \tag{6}$$

2.2 Equation of Motion : Nonlinear (Hertzian)

The equation of motion for any particle i (except the boundary particles at either end of the chain) by using Eq. (3), (4) and non-dimensionalization (Sect. 2.1) can be written as

$$b^{(i)} \frac{\mathrm{d}^2 u^{(i)}}{\mathrm{d}t^2} = F_{(i-1,i)} + F_{(i,i+1)} = \kappa_{(i-1,i)} \delta_{(i-1,i)}^{1+\beta} - \kappa_{(i,i+1)} \delta_{(i,i+1)}^{1+\beta}, \tag{7}$$

which can also be written as

$$b^{(i)} \frac{\mathrm{d}^2 u^{(i)}}{\mathrm{d}t^2} = \kappa_{(i-1,i)} \left[\Delta_{(i-1,i)} - (u^{(i)} - u^{(i-1)}) \right]^{(1+\beta)} - \kappa_{(i+1,i)} \left[\Delta_{(i+1,i)} - (u^{(i+1)} - u^{(i)}) \right]^{(1+\beta)}. \tag{8}$$

For particles interacting repulsively with Hertzian potential, $\beta = 1/2$, Eq. (7) or (8) can be solved numerically, see Sect. 3.1.

2.3 Equation of Motion : Linear

The repulsive interaction force can be expressed as a power series and can be expanded about the initial overlap $\Delta_{(i,j)}$ due to pre-compression,

$$F_{(i,j)} = \kappa_{(i,j)} \Delta_{(i,j)}^{1+\beta} + \kappa_{(i,j)} (1+\beta) \Delta_{(i,j)}^\beta (\delta_{(i,j)} - \Delta_{(i,j)}) + \frac{1}{2} \kappa_{(i,j)} \beta(1+\beta) \Delta_{(i,j)}^{\beta-1} (\delta_{(i,j)} - \Delta_{(i,j)})^2 + \dots \tag{9}$$

For small displacements from the equilibrium condition (during wave propagation), using the definition of $\delta_{(i,j)}$ and after ignoring higher order non-linear terms, we arrive at

$$F_{(i,j)} = \kappa_{(i,j)} \Delta_{(i,j)}^{1+\beta} - \kappa_{(i,j)} (1+\beta) \Delta_{(i,j)}^\beta \left(u^{(j)} - u^{(i)} \right). \tag{10}$$

Inserting the force relation (Eq. (10)) in Eq. (7), we get the general, linearized equation of motion:

$$b^{(i)} \frac{\mathrm{d}^2 u^{(i)}}{\mathrm{d}t^2} = \kappa_{(i-1,i)} \Delta_{(i-1,i)}^\beta \left[\Delta_{(i-1,i)} - (1+\beta)(u^{(i)} - u^{(i-1)}) \right] - \kappa_{(i+1,i)} \Delta_{(i,i+1)}^\beta \left[\Delta_{(i+1,i)} - (1+\beta)(u^{(i+1)} - u^{(i)}) \right]. \tag{11}$$

For Hertzian nonlinear repulsive interaction force between the particles, the scaled stiffness $\kappa_{(i,j)}$ and initial overlap $\Delta_{(i,j)}$ are given as follows (see Appendix B for details):

$$\kappa_{(i,j)} = \sqrt{\frac{2}{b^{(i)1/3} + b^{(i)1/3}}} (b^{(i)} b^{(j)})^{1/6}, \tag{12}$$

and

$$\Delta_{(i,j)} = \kappa_{(i,j)}^{(-2/3)}. \tag{13}$$

The Hertzian nonlinear repulsive interaction force is appropriate for spherical particles (Landau and Lifshitz (1970)). Eq. (11) can be written in a linearized form as

$$\frac{b^{(i)}}{(1+\beta)}\frac{\mathrm{d}^2 u^{(i)}}{\mathrm{d}t^2} = \kappa_{(i+1,i)}^{1/(1+\beta)}(u^{(i+1)} - u^{(i)}) - \kappa_{(i-1,i)}^{1/(1+\beta)}(u^{(i)} - u^{(i-1)}) \tag{14}$$

Since, we are interested only in mass disorder, we can choose all coupling stiffness ($\kappa_{(i,j)}$) as 1. Now, Eq. (14) for individual particles can be written as

$$\frac{b^{(i)}}{(1+\beta)}\frac{\mathrm{d}^2 u^{(i)}}{\mathrm{d}t^2} = u^{(i+1)} - 2u^{(i)} + u^{(i-1)} \tag{15}$$

The factor $\frac{1}{1+\beta}$ becomes 1 for the linear contact model ($\beta = 0$) and it becomes 2/3 for the Hertzian contact model ($\beta = 1/2$). It can be observed that the factor $\frac{1}{1+\beta}$ has only multiplicative influence on the physical parameters. Since, in our system of equations (Eq. (15)) only mass disorder is present, the masses of the particles get multiplied by this factor ($\frac{1}{1+\beta}$). For further analysis, $\beta = 0$ has been chosen so that

$$b^{(i)}\frac{\mathrm{d}^2 u^{(i)}}{\mathrm{d}t^2} = u^{(i+1)} - 2u^{(i)} + u^{(i-1)} \tag{16}$$

This results in N equations which eventually can be expressed in matrix form:

$$\mathbf{M}\frac{\mathrm{d}^2\mathbf{u}}{\mathrm{d}t^2} = \mathbf{K}\mathbf{u} + \mathbf{f}, \tag{17}$$

where $\mathbf{M}$ is a diagonal mass matrix with entries $b^{(1)}, b^{(2)}, b^{(3)}, ..., b^{(N)}$ and zero otherwise; $\mathbf{K}$ is a matrix with diagonal entries $-(\kappa_{(i+1,i)} + \kappa_{(i-1,i)}) = -2$, superdiagonal ($\kappa_{(i+1,i)}$) and subdiagonal ($\kappa_{(i-1,i)}$) entries +1 and zero otherwise for $\kappa = 1$. $\mathbf{f}$ is the external force which depends on the specified driving. Introducing, $\mathbf{A} = -\mathbf{M}^{-1}\mathbf{K}$ then, Eq. (17) can be written as

$$-\frac{\mathrm{d}^2\mathbf{u}}{\mathrm{d}t^2} = \mathbf{A}\mathbf{u} - \mathbf{M}^{-1}\mathbf{f}. \tag{18}$$

2.4 Analysis in real space/spatial Fourier space :

Using an ansatz for real space and another ansatz for spatial Fourier space in Eq. (18) (the calligraphic fonts from now onwards will depict the spatial Fourier transform counterparts of the real space parameters),

$$\mathbf{u} = \mathbf{u}'e^{i\omega t} \quad \text{or} \quad \mathcal{U} = \mathcal{U}'e^{i(\omega t - ku)}, \tag{19}$$

one has

$$\mathbf{A}\mathbf{u} = \omega^2\mathbf{u} \quad \text{or} \quad \mathbf{A}\mathcal{U} = \omega^2\mathcal{U}, \tag{20}$$

where k is the wavenumber and $\mathcal{U} = \int\limits_{-\infty}^{\infty} \int\limits_{-\infty}^{\infty} u e^{-i(\omega t - ku)} \mathrm{d}t \, \mathrm{d}u$ is the double Fourier transform (spatial as well as temporal) ansatz. Equation (20) is a familiar eigen value problem. The eigenvalues ω_j^2 and eigenvectors $\mathbf{s}_{(j)}$ of the matrix $\mathbf{A}$ give the eigendomain of the granular chain that are independent of the external driving. The square roots of the eigenvalues, ω_j, are the natural frequencies of the chain. The set of eigenvectors can be orthonormalised to obey the orthonormality condition:

$$\mathbf{s}_{(i)}^{\mathrm{T}} \mathbf{M} \mathbf{s}_{(j)} = \delta_{ij}, \tag{21}$$

with δ_{ij} being the Kronecker delta symbol. The $\mathbf{S}$ matrix or the eigenbasis matrix can be constructed with $\mathbf{s}_{(j)}$ as the columns of the matrix, which can be used to transform back and forth from real domain to eigen domain. The columns ($\mathbf{s}_{(j)}$) of the matrix $\mathbf{S}$ are sorted such that the corresponding eigenvalues ω_j are in increasing order. The vector of eigenmode amplitudes is

$$\mathbf{z} = \mathbf{S}^{-1} \mathbf{u} \quad \text{or} \quad \mathcal{Z} = \mathbf{S}^{-1} \mathcal{U}. \tag{22}$$

10 A matrix $\mathbf{G}$ consisting of eigenvalues ω_j along the diagonal (in increasing order) is formulated such that $\mathbf{G} = \mathbf{S}^{-1} \mathbf{A} \mathbf{S}$ which allows the transformation of Eq. (17) into the eigendomain as

$$\frac{\mathrm{d}^2 \mathbf{z}}{\mathrm{d}t^2} = -\mathbf{G}\mathbf{z} + \mathbf{S}^{-1}\mathbf{M}^{-1}\mathbf{f} = -\mathbf{G}\mathbf{z} + \mathbf{h} \quad \text{or} \quad \frac{\mathrm{d}^2 \mathcal{Z}}{\mathrm{d}t^2} = -\mathbf{G}\mathcal{Z} + \mathbf{S}^{-1}\mathbf{M}^{-1}\mathcal{F} = -\mathbf{G}\mathcal{Z} + \mathcal{H}, \tag{23}$$

which defines h and $\mathcal{H}$ implicitly. The differential equations (23) are decoupled and can be solved to give

$$\mathbf{z}(t) = \mathbf{C}^{(1)}\mathbf{a} + \mathbf{C}^{(2)}\mathbf{b} + \mathbf{z}_P(t) \quad \text{or} \quad \mathcal{Z}(t) = \mathbf{C}^{(1)}\mathcal{A} + \mathbf{C}^{(2)}\mathcal{B} + \mathcal{Z}_P(t) \tag{24}$$

15 where $\mathbf{C}^{(1)}$ is a diagonal matrix with $\mathbf{C}_{j,j}^{(1)} = \sin(\omega_j t)$, $\mathbf{C}^{(2)}$ is a diagonal matrix with $\mathbf{C}_{j,j}^{(2)} = \cos(\omega_j t)$, and $\mathbf{z}_P(t)$ or $\mathcal{Z}_P(t)$ are the particular solutions of the differential equations, which depend on $\mathbf{h}$ or $\mathcal{H}$ and, hence, depend on the external driving force $\mathbf{f}$ or $\mathcal{F}$. The vectors $\mathbf{a}$ or $\mathcal{A}$ and $\mathbf{b}$ or $\mathcal{B}$ are determined by the initial conditions from the initial displacement ($\mathbf{u}_o$ or $\mathcal{U}_o(k)$) and velocities ($\mathbf{v}_o$ or $\mathcal{V}_o(k)$).

$$\mathbf{b} = \mathbf{S}^{-1}\mathbf{u}_o - \mathbf{z}_P(0) \quad \text{or} \quad \mathcal{B} = \mathbf{S}^{-1}\mathbf{u}_o - \mathbf{z}_P(0) \tag{25}$$

20 and

$$\mathbf{a} = \mathbf{G}^{-1}\mathbf{S}^{-1}\mathbf{v}_o - \mathbf{G}^{-1}\frac{\mathrm{d}\mathbf{z}_P(t)}{\mathrm{d}t}\bigg|_{t=0} \quad \text{or} \quad \mathcal{A} = \mathbf{G}^{-1}\mathbf{S}^{-1}\mathcal{V}_o - \mathbf{G}^{-1}\frac{\mathrm{d}\mathcal{Z}_P(t)}{\mathrm{d}t}\bigg|_{t=0} \tag{26}$$

$\mathbf{a}$ and $\mathbf{b}$ or $\mathcal{A}$ and $\mathcal{B}$ are column vectors with column elements a_j and b_j or $\mathcal{A}_j$ and $\mathcal{B}_j$, associated with a particular eigenfrequency (ω_j). The solution in real space can be obtained by the transformation mentioned in Eq. (22) which can be applied on Eq. (24) to give

$$\mathbf{u}(t) = \mathbf{S}\mathbf{C}^{(1)}\mathbf{a} + \mathbf{S}\mathbf{C}^{(2)}\mathbf{b} + \mathbf{u}_P(t) \quad \text{or} \quad \mathcal{U}(t) = \mathbf{S}\mathbf{C}^{(1)}\mathcal{A} + \mathbf{S}\mathbf{C}^{(2)}\mathcal{B} + \mathcal{U}_P(t). \tag{27}$$

2.5 Initial Conditions : Impulse Driving

The initial conditions required to solve various special cases are the initial displacements ($\mathbf{u}_o$) and initial velocities ($\mathbf{v}_o$) in real space and $\mathcal{V}_o$ and $\mathcal{U}_o$ in spatial Fourier space. Besides the sinus driving used in Lawney and Luding (2014), we apply impulse driving initial condition. For an impulse driving mode, the boundary conditions are as follows:

$$u^{(i)}(t=0) = 0, \ v^{(i \neq 1)}(t=0) = 0, \ v^{(1)}(t=0) = v_o. \tag{28}$$

An impulse driven chain has an impulse imparted to the first particle, $i = 1$ with initial velocity v_o. Since the focus of our study is not on the occurrence of sonic vacuum (Nesterenko (1983)), the initial impulse (v_o) should be chosen small enough to avoid opening of contacts. Using Eq. (27), (25), (26) and the initial conditions for the impulse driven chain i.e. $\mathbf{f} = 0$ (no driving present), $\mathbf{u}_o = 0$ and $\mathbf{v}_o = [v_o \ 0 \ldots 0]^{\mathrm{T}}$, we get

$$\mathbf{a} = \mathbf{G}^{-1}\mathbf{S}^{-1}\mathbf{v}_o \quad , \quad \mathbf{b} = 0, \tag{29}$$

and

$$\mathbf{u} = \mathbf{S}\mathbf{C}^{(1)}\mathbf{G}^{-1}\mathbf{S}^{-1}\mathbf{v}_o \quad \& \quad \mathbf{v} = \mathbf{S}\mathbf{C}^{(2)}\mathbf{S}^{-1}\mathbf{v}_o, \tag{30}$$

which implies that displacements and velocities of all particles p are given analytically by

$$u^{(p)}(t) = v_o \sum_{j=1}^{N} \frac{S_{pj}S_{1j}\sin(\omega_{(j)}t)}{\omega_{(j)}} \quad \& \quad v^{(p)}(t) = v_o \sum_{j=1}^{N} S_{pj}S_{1j}\cos(\omega_{(j)}t). \tag{31}$$

In wavenumber space (spatial Fourier transform), the initial condition is specified by $\mathcal{V}_o(k)$ which can be a sine or cosine function in terms of wavenumber (k). Using Eq. (27) and $\mathcal{V}_o(k)$, we get

$$\mathcal{A} = \mathbf{G}^{-1}\mathbf{S}^{-1}\mathcal{V}_o(k) \quad , \quad \mathcal{B} = 0, \tag{32}$$

and thus,

$$\mathcal{U} = \mathbf{S}\mathbf{C}^{(1)}\mathcal{A} \quad \& \quad \mathcal{V} = \mathbf{S}\mathbf{C}^{(2)}\mathbf{G}\mathcal{A}, \tag{33}$$

2.6 Mass Distribution, Disorder Parameter (ξ), Ensemble Averaging & Binning

The mass distribution of the monodisperse chain has been selected randomly from normal ($f^{(n)}(b)$), uniform ($f^{(u)}(b)$) and binary ($f^{(bi)}(b)$) distributions whose standard deviations give the measure of the disorder of mass in the chain (ξ). For instance, the normal distribution is given by

$$f^{(n)}(b) = \frac{1}{\xi\sqrt{2\pi}}e^{\frac{(b-1)^2}{2\xi^2}}. \tag{34}$$

High disorder means that the difference between the lightest particle and the heaviest particle is very large. It was observed in Lawney and Luding (2013) that the three distributions showed quantitatively similar behavior if the first two moments of

the distributions were the same. Here, the first two moments of the aforementioned three distributions have been matched. The mathematical details of the distributions are given in Appendix C. Ensembles of chains with different realizations for a particular disorder and distribution have been taken into consideration. Angular brackets will be used to denote ensemble averaged physical quantities like $\langle \mathbf{u} \rangle$, $\langle E_{tot} \rangle$, etc. The first five moments of the three distributions for different disorder (standard deviation) $\xi = 0$, $\xi = 0.1$, $\xi = 0.2$, $\xi = 0.35$, $\xi = 0.5$ and $\xi = 0.8$ are given in Table 1 (500 ensembles scaled), Table 2 (500 ensembles unscaled) and Table 3 (10000 ensembles).

2.7 Participation Ratio & Localization Length

The participation ratio (P_j) (introduced in Bell and Dean (1970) and used previously in Allen and Kelner (1998), Zeravcic et al. (2009)) is a crucial tool in determining the localization length ($\tilde{L}_j$) associated with a particular eigenmode. This localization length can be seen as the length beyond which elastic waves with a particular frequency become evanescent, i.e., they decay exponentially in a disordered system (Mouraille (2009)). It is instrumental in determining the length within which the elastic waves become confined in space and is dependent on the frequency and thus the eigenmode (Anderson (1958)). The participation ratio of eigenmode j is defined as

$$P_j = \frac{1}{\sum\limits_{i=1}^{N} (S_{ij})^4} \tag{35}$$

with the normalization condition on the eigenmodes $\sum\limits_{i=1}^{N} (S_{ij})^2 = 1$. For one dimension, the localization length is defined as $\tilde{L} = P_j \tilde{d}$ where $\tilde{d}$ is the particle center distance in equilibrium, i.e. under pre-compression. The localization length can now be non-dimensionalised by the internal particle scale of separation $\sim \tilde{d}$ to give $L_j \cong P_j$. As discussed and pointed out in Allen and Kelner (1998), the localization length of the lowest eigenmode is often attributed to the length of the chain (which would be regarded as a force chain in our analysis) and hence, it becomes important to find the localization length of an ordered chain, $\xi = 0$ as reference. For an ordered chain $b^{(1)}, b^{(2)}, b^{(3)}, ..., b^{(N)} = 1$ and $\kappa = 1$, so,

$$\mathbf{A} = \begin{bmatrix} -2 & 1 & 0 & 0 & \cdots & 0 \\ 1 & -2 & 1 & 0 & \cdots & 0 \\ 0 & 1 & \ddots & 0 & \cdots & 0 \\ 0 & \cdots & 0 & \ddots & 0 & 1 \\ 0 & \cdots & 0 & 0 & 1 & -2 \end{bmatrix} \tag{36}$$

The eigenvalues of this matrix are $\omega_j^2 = 4\sin^2\left(\frac{j\pi}{2N}\right)$ and its eigenvectors are $\mathbf{s}_{(j)} = \{\sin\left(\frac{j\pi}{N}\right), \sin\left(\frac{2j\pi}{N}\right), \sin\left(\frac{3j\pi}{N}\right)...\sin\left(\frac{(N-1)j\pi}{N}\right)\}$. After respecting the normalization condition and the definition of the participation factor, the localization length of the lowest eigenmode (P_1) can be analytically calculated from the eigenvectors

as

$$P_{norm} = \sum_{i=1}^{N} \sin\left(\frac{ij\pi}{N}\right)^2, \text{ and hence, } P_j = \frac{P_{norm}^2}{\sum\limits_{i=1}^{N}\left(\sin\left(\frac{ij\pi}{N}\right)\right)^4} \tag{37}$$

For $N = 256$, $P_1 = 170.667 \approx 171$.

2.8 Dispersion

5 The analytical expression for the dispersion relation in an ordered chain of particles/elements with linear contact forces are given by (Brillouin (1946), Tournat et al. (2004), Lawney and Luding (2014))

$$\tilde{\omega}^2 = 4\frac{\tilde{\kappa}_o}{\tilde{M}_1}\sin^2\left(\frac{\tilde{k}\tilde{d}}{2}\right), \tag{38}$$

where the wavenumber can be non-dimensionalized by the microscopic particle scale of separation ($\tilde{d}$) and frequency by $\sqrt{\frac{\tilde{\kappa}_o}{\tilde{M}_1}}$ giving the non-dimensional dispersion relation:

10 $$\omega^2 = \Omega_\pi^2 \sin^2\left(\frac{k}{2}\right), \tag{39}$$

with $\Omega_\pi = 2$ for ordered chains with $\xi = 0$. Eq. (39) holds for propagative as well as evanescent waves. The positive roots of this relation correspond to propagative waves and the imaginary roots to evanescent waves (Tournat et al. (2004)). This expression also holds for longitudinal wave propagation in 3D granular packings (Mouraille and Luding (2008)) and in 1D chains (Lawney and Luding (2014)). From the dispersion relation, it can be noted that disorder creates a maximum permissible

15 frequency (Ω_π) for propagating waves, frequencies below Ω_π are propagative and the frequencies above Ω_π are evanescent. The dispersion relation (Eq. (39)) for ordered chains ($\xi = 0$) is

$$\omega = 2\sin\left(\frac{k}{2}\right), \tag{40}$$

which is the dispersion relation for propagative waves.

2.9 Total Energy Dispersion

20 From Eq. (A5) it can be observed that the total energy of the eigenmodes is constant with respect to time as given by

$$E_{tot}(\omega_j, k) = \frac{1}{2}\mathcal{A}_j(k)^2\omega_j^2. \tag{41}$$

By taking the first moment of this eigenmodal total energy representation about frequency, a dominant frequency related to a particular wavenumber can be obtained. Moments of the eigenmodal total energy representation are defined as

$$M^{(m)}(k) = \frac{\sum \omega_j^m E_{tot}(\omega_j, k)}{E_{tot}(\omega_j, k)}. \tag{42}$$

25 The dominant frequency is given by the first moment,

$$\Omega(k) = M^{(1)}(k) = \frac{\frac{1}{2}\sum\limits_j \mathcal{A}_j^2\omega_j^3}{E_{tot}}. \tag{43}$$

The dominant frequency can be measured by averaging over all eigenmodes for a single realization with $\mathcal{A}_j(k)$ as a multiplicative factor which depends on the Fourier initial condition $\mathcal{V}_o(k)$ (Eq. (32)). The dispersion relation for the propagating waves can be obtained by taking ensemble averages of this dominant frequency ($\langle\Omega(k)\rangle$), which will be plotted in Fig. 10(b) below for different disorder strengths (500 ensembles).

2.10 Group velocity

The group velocity is given by

$$v_g = \frac{\partial\omega}{\partial k},\tag{44}$$

for both propagative waves and evanescent waves. It can be obtained by differentiating Eq. (40) that

$$v_g(k) = \frac{\sqrt{\Omega_\pi^2 - \omega^2}}{2}.\tag{45}$$

where $\Omega_\pi = \Omega_\pi(\xi)$ depends on disorder as we will see below.

3 Results & Discussions

The analytical expressions derived in the previous sections are computed for $N = 256$ particles long chains. The impulse imparted to the first particle is $v_o = 0.05$. The time step utilized for the output is, $\Delta t = 0.0312$ and the maximum time up to which the computations have been carried out is $t_{max} = 256$ such that the pulse has just about reached the 256th particle. As it can be seen from Tables 1 and 3, the scaled average mass of the particles has been kept $M_1 = 1$ and $\xi = 0.0, 0.1, 0.2, 0.35, 0.5$ and 0.8 disorder parameters (standard deviation; see appendix) have been used for analysis. Using the analytical solution of the linearized system (Eq. (31)), ensembles of 500 and 10000 chains along with representative single realizations will be shown in this section.

3.1 Nonlinear (Hertz) and Linear Space Time Responses

Equation (8) with Eq. (12) and Eq. (13) has been solved numerically with Verlet integration to get space time responses of particles having nonlinear (Hertzian) repulsive interaction force. The time step used for the numerical integration is $\Delta t = 0.00038147$. Fig. 3 shows the space time responses calculated numerically for the nonlinear equation of motion (Eq. (8)) and the space time responses calculated for the linearized equation of motion (Eq. (14)) using a small initial velocity $v_o = 0.05$. The space time responses are obtained for a single realization of a granular chain without ensemble averaging. The nonlinear space time responses coincide with the linear space time responses, confirming that the solution given by Eq. (31) is also appropriate for particles with nonlinear repulsive interaction forces for small displacements.

In order to observe the limitation of the linear space time responses obtained from Eq. (31), Fig. 4 is plotted. The difference between the maximum value (u_{peak}) of the space time responses for Hertzian and linear repulsive interaction force ($u_{\text{diff}}^{(p)} = u_{\text{peak(hertz)}}^{(p)} - u_{\text{peak(linear)}}^{(p)}$) is chosen as a parameter to judge the appropriateness of linear space time response for the nonlinear
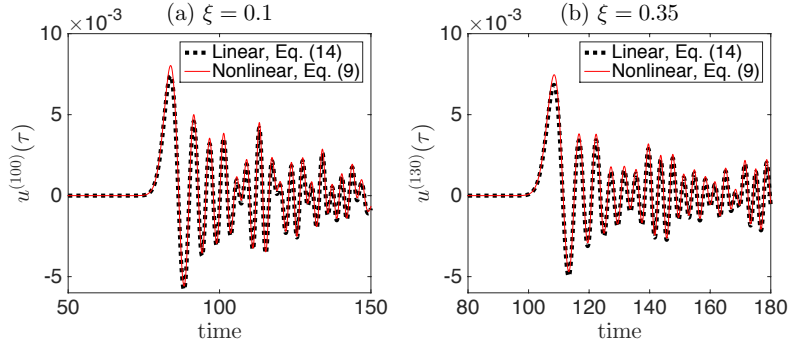
Figure 3. The displacement as a function of time is shown for the 100th particle in a chain of particles with disorder parameter $\xi = 0.1$ in (a) and the 130th particle in a chain of particles with disorder parameter $\xi = 0.35$ in (b) and $v_o = 0.05$.
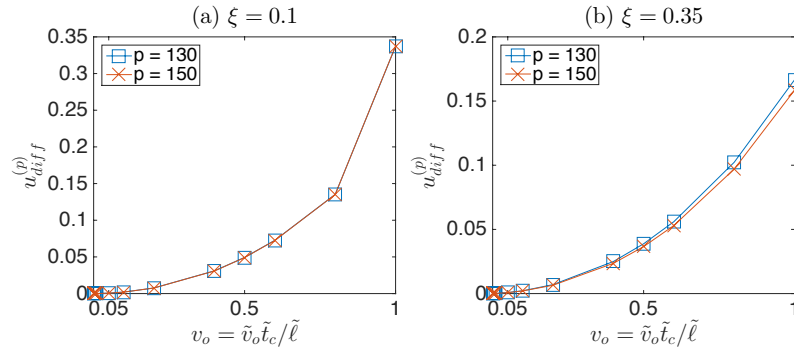
Figure 4. The nonlinear increase in $u_{\text{diff}}^{(p)}$ (a parameter which shows dissimilarity between linear and nonlinear space time responses) with initial impulse velocity (v_o). The value $v_o = 0.05$ is in the zone where linear and nonlinear space time responses are almost identical.

equation of motion (Eq. (8)). The difference between nonlinear (Hertz) and linear space time response increases nonlinearly irrespective of particle position and disorder parameter of the granular chain.

3.2 Displacement Response of three mass distributions

The mass disorder of the particles in the chain with length 256 is taken into consideration only and κ is chosen as 1 (Sect. 2.3). Figure 5 shows the displacement as a function of time of the 150th particle (Fig. 1(a) & 1(c)) and of the 220th particle (Fig. 1(b) & 1(d)), which are placed before and after the reference localization length (the maximum possible, $L_{max} = 171$, Sect. 3.7) for two disorder parameters $\xi = 0.1$ and $\xi = 0.5$ with three mass distributions (normal, uniform and binary). For weak disorder ($\xi = 0.1$), it is observed that the displacement wave packets are perfectly superposed affirming what was concluded in Lawney and Luding (2013) & Lawney and Luding (2014) that the shape of the distribution has no effect on the propagating pulse if the first two moments of the distribution are the same (Table 1). For stronger disorder ($\xi = 0.5$), the wave packets are not collapsing perfectly (Fig. 1(c) & 1(d)). As it can be seen in Table 1 there is a numerical mismatch between the unscaled moments of the
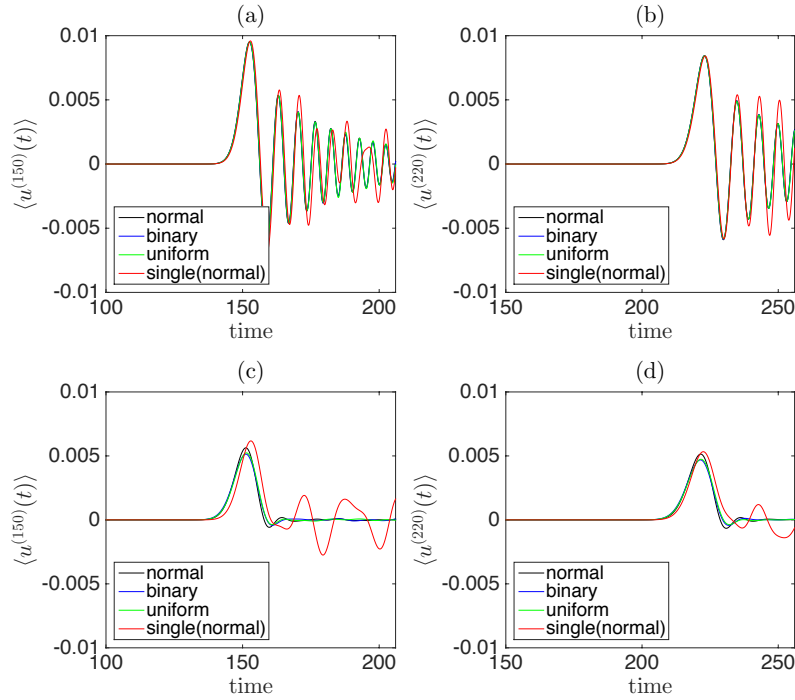
Figure 5. Ensemble averaged displacements (500 times) of 150th ((a) and (c)) and 220th ((b) and (d)) particle with respect to time. (a) and (b) have disorder parameter $\xi = 0.1$, (c) and (d) have disorder parameter $\xi = 0.5$. The red plot is the space time response from a single realization of a chain with normally distributed masses. $\forall$ single realization, normal distribution is used with $\tilde{M}_1 = 0.9971$ and $\tilde{M}_2 = 1.1274$ for $\xi = 0.1$, $\tilde{M}_1 = 0.9971$ and $\tilde{M}_2 = 1.1274$ for $\xi = 0.5$ and $\tilde{M}_1 = 0.9958$ and $\tilde{M}_2 = 1.2636$ for $\xi = 0.5$

distributions leading to a dissimilarity between the second scaled moments ($\langle M_2 \rangle$). This also causes the real standard deviation (disorder; ξ) which has been numerically calculated (Ξ; Table 1) to deviate a little bit from it's intended value. It can also be observed from Fig. 5 (c) and (d) that the pulse shapes of binary distribution and uniform distribution are closer to each other in comparison to normal and binary or normal and uniform, since, the scaled second moments ($\langle M_2 \rangle$) of binary and uniform distributions for $\xi = 0.5$ are closest to each other (Table 1). Similar conclusions about similarity, dissimilarity and closeness can be drawn about pulse shapes of different distributions for different disorder parameters (ξ (intended), Ξ (numerically obtained)) on the basis of moments of the mass distribution. For larger ξ, higher moments (as listed in Tables 1, 2 and 3) have to be considered (Ogarko and Luding (2013)), but discussing these higher moments and their consequences go beyond the scope of this study.

3.3 Displacement Response for Different Disorder Parameters (ξ)

Mechanical waves propagating through disordered media or granular media like soil (on the receiver end) can be divided into two parts, the coherent part and the incoherent part (Jia et al. (1999), Jia (2004)). The coherent part is the leading wave packet and self averaging in nature (it maintains its shape after ensemble averaging) and it is used for determining the bulk sound wave velocity. In contrast, the incoherent part is the scattering, non-self averaging part, which is strongly system configuration dependent, also known as coda or tail of the mechanical wave. Figure 6 contains the displacement of the same particles (150th & 220th particles) used in subsection 3.2 for consistency. Here, attention has been given to the effect of the mass distribution on the time of arrival/flight and hence, the wave velocity of the initial wave packet. Figures 6(a) and 6(b) contain the displacements of the 150th and 220th particle (before and after L_{max}, Sect. 3.7) for single realizations, 500 ensembles and 10000 ensembles. The leading wave packet is the same for 500 ensembles and 10000 ensembles in both figures, i.e. the coherent part of the wave which maintains its shape after averaging. The coda is more or less pronounced at 150 or 220, respectively and vanishes due to ensemble averaging. Figures 6(c) and 6(d) show the displacement response of the 150th and the 220th particle with respect to time for chains with different mass disorder. The speed of the coherent wave packet (from source to receiving particle, peak of signal) is increasing with disorder. Higher disorder leads to higher coherent wave (peak) speed, irrespective of the localization length (L_{max}). However, this increase in wave speed can also be attributed to sound wave accaleration near the source as pointed out by Mouraille et al. (2006) and may not be generalized as effect of mass disorder in the chain, as investigated in the next section.

3.4 Coherent Wave Speed and Disorder

Table 4 and Fig. 7 contain the velocity of the peak of the coherent wave, the velocity of the rising part of the coherent wave packet when the displacement of the particle has attained 5%, 10%, 70%, 90% of the peak value and the first time when the displacement of the particle becomes 0 after it has attained the peak value of the coherent wave (zero crossing), all constituting the coherent wave packet. The velocities were determined through velocity picking (particle position divided by the time of arrival). The particles used for computing the velocities were 130, 150, 200 and 220 (Table 4; 2 before localization length and 2 after localization length, $L_{max} = 171$). It can be observed that irrespective of the rising part of the coherent wave packet (5%, 10%, of the peak value etc.) and the peak (Fig. 7(a), (b), (c), (d)), the wave velocity increases with disorder. However, for zero crossing (Fig. 7(e)), the velocity decreases with increase in disorder and the same can be said for the part of the coherent wave packet which lies after the peak value, this can be attributed to the increased spreading of the wave packet with increase in disorder. Notably, the speed measured at particle 130 is larger/smaller if the earlier/later parts of the signal are considered. Fig. 7(f) shows the velocity of the peak value of the coherent wave packet of all the particles of the granular chain for different disorder parameters and it also exhibits a similar kind of acceleration of signal/mechanical wave near the source as was observed in Mouraille et al. (2006). This acceleration is caused by self-demodulation of the initial impulse imparted to the granular chain and the noteworthy point is that the acceleration increases with increase in disorder. However, due to this observation we cannot generalize the effect of disorder on wave speed. The sudden rise in velocity of the peak value in
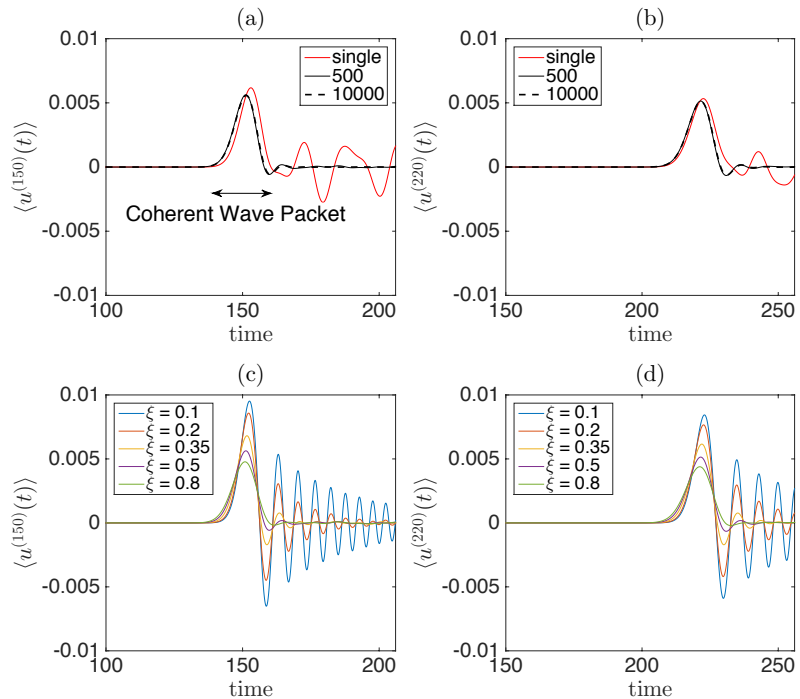
Figure 6. Displacements of 150th ((a) and (c)) and 220th ((b) and (d)) particle with respect to time for different ensembles ((a) and (b)) of disorder $\xi = 0.5$ and of multiple disorder parameters ((c) and (d); for 500 ensembles).

Fig. 7(f) after the 250th particle is due to the boundary effect as well as due to the presence of the coherent wave front of the traveling wave around that position as the maximum time window used is $t_{max} = 256$. For practical purposes, we remark the wave speed measured varies by a few percent up and down, dependent on which part of the signal is used for measurement.
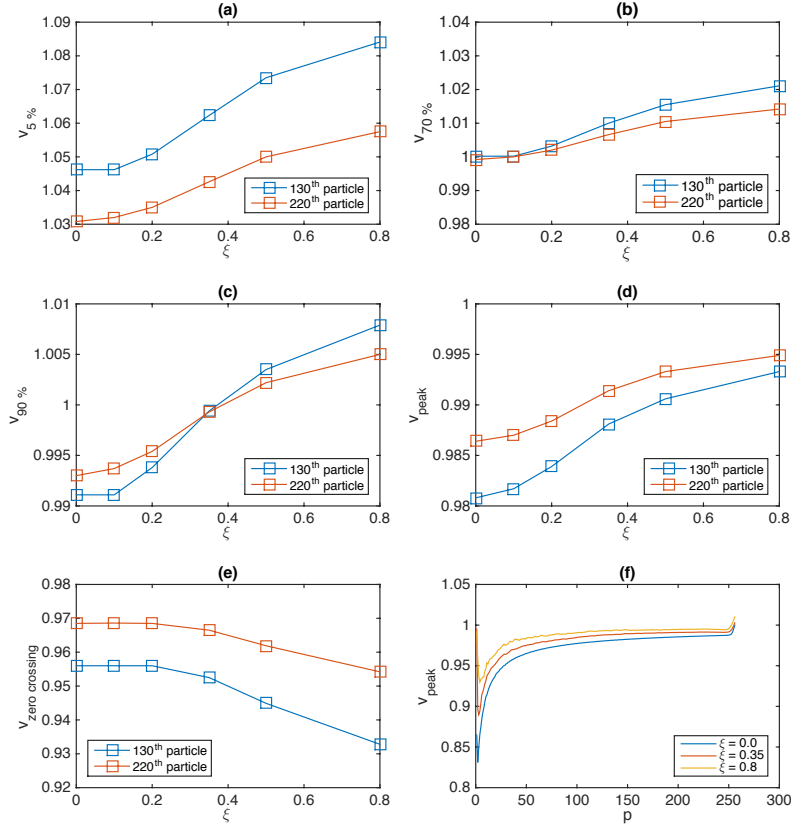
Figure 7. Coherent Wave Velocities determined through Velocity picking. The peak of the coherent wave packet's velocity ((d)) and the rising part of the packet ((a), (b) and (c)) as well as the falling part ((e)) are taken into consideration. (f) plots the peak velocity for all the particles in a granular chain with different ξ. Note that (a), (b) and (e) have a different axis range as (c) and (d).

To understand the effect of disorder on wave speed without taking into account this "source effect", the velocity based on the time taken by the pulse for propagating a common distance of 7 particles has been computed in Table 6 and the results have been plotted in Fig. 8. The reason for selecting such a low common distance of separation was to keep the effect of the source as minimal as possible; the sets of points (130 to 137, 150 to 157, 220 to 227 and 240 to 247 particles) were used with different reference points of the coherent wave front (5%, 10%, 70%, 90%, peak value and zero crossing). From Fig. 8 and Table 6 it can be observed that follow the same trend, except the velocity computed using the zero crossing reference point, which are more or less constant with little fluctuations (Table 6). Fig. 8(a) shows a consistent increase of velocity as it is the closest to the source (dominated by the source effect), however, as the set of particles is selected farther away from the source, the velocity trend shows a slight decrease and then an increase with increasing ξ (Fig. 8(b) and (c)). Fig. 8(d) exhibits a consistent decrease
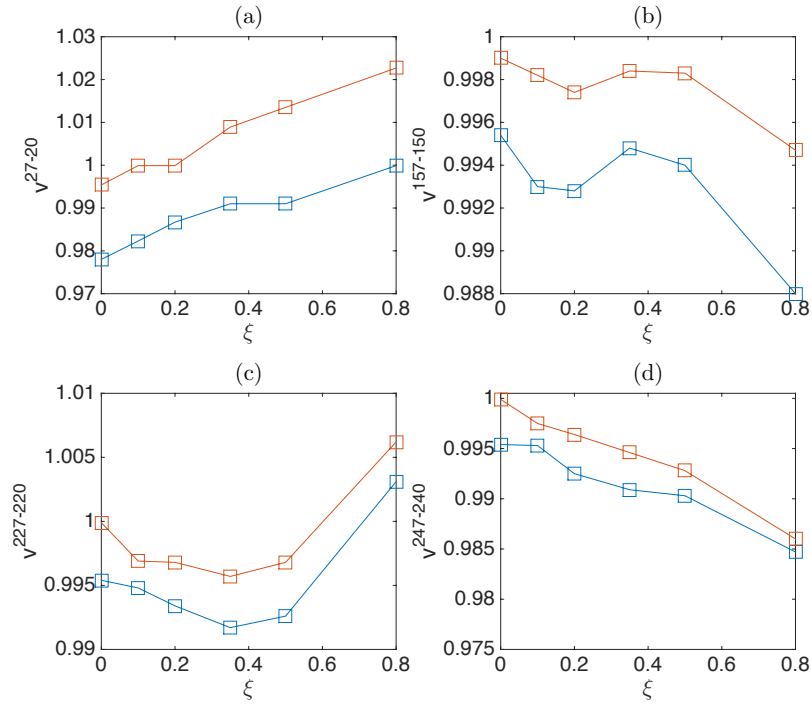
Figure 8. Wave speed for common distance of separation (7 particles/elements) with different disorder ξ.

of velocity with increase in ξ because the set of particles (247-240) are far from the source (source effect is weak). From Fig. 8(d), it can be interpreted that higher disorder results in decrease in wave velocity.

3.5 Frequency Response & Dispersion

In Fig. 9(a) & Fig. 9(c) a Fast Fourier Transform (FFT) with respect to time is carried out on the displacement response of a 256 element long chain for disorder, $\xi = 0.01$ and $\xi = 0.35$, respectively (when an impulse of $v_o = 0.05$ has been applied to the first particle) to observe the frequency content with distance, (the sampling frequency is $\omega_{sample} = \frac{2\pi}{\Delta t}$) and responses upto half of the sampling frequency were taken into account to avoid aliasing (Nyquist criterion). The first 5 particles have been excluded from the Fourier transform to avoid an overwhelming driving signal effect. Fig. 9(a) exhibits the existence of cut-off frequency ($\omega = 2$) above which the waves become evanescent. The bending of the intensity with distance (particle number), especially at large distances, is attributed to dispersion and the finite time window. Using the group velocity (p is the particle number)

$$v_g t_{max} = p, \tag{46}$$

for an ordered chain ($\xi = 0$), $\Omega_\pi = 2$ and using Eq. (45), the frequency envelope is

$$\omega(p) = 2\sqrt{1 - \frac{p^2}{t_{max}^2}}, \tag{47}$$

which is the red curve plotted in Fig. 9(a).

A spatial as well as temporal 2D FFT is carried out for a single realization of a 256 element long chain with disorder $\xi = 0.01$ and $\xi = 0.35$ to observe the dispersion relation (Fig. 9(b) & 9(d); ω v/s k). 2D FFT has been used previously for one-dimensional and three dimensional polydisperse granular packings for obtaining dispersion relations (Luding and Mouraille (2008), Lawney and Luding (2014), O'Donovan et al. (2015)) but strong frequency filtering due to the disordered system resulted in ambiguous dispersion relations (flat bands and absence of certain frequencies below the cut-off frequency, which indicates the non-propagative bands due to the presence of defect modes). This can also be observed from Fig. 9(b) and Fig. 9(d). Eq. (40) (the dispersion relation for an ordered chain) has been plotted in Fig. 9(b) which gives a perfect fit for the denser regime in the figure. However for the disordered chain, $\xi = 0.35$, as proposed earlier in Sect. 2.9, the dispersion relation is better given by $\langle \Omega(k) \rangle$ by ensemble averaging the dominant frequencies with respect to different wavenumbers. $\langle \Omega(k) \rangle$ for 500 ensembles with disorder $\xi = 0.35$ has been plotted in Fig. 9(d) (the green curve). For low frequencies the green curve perfectly superposes the dense regime in the displacement's temporal and spatial Fourier transform; for higher frequency ($\omega \rangle 1.5$) due to the appearance of a flat band (defect mode) the intensity is not present near the green curve, which holds true for low and intermediate frequencies/wavenumbers.
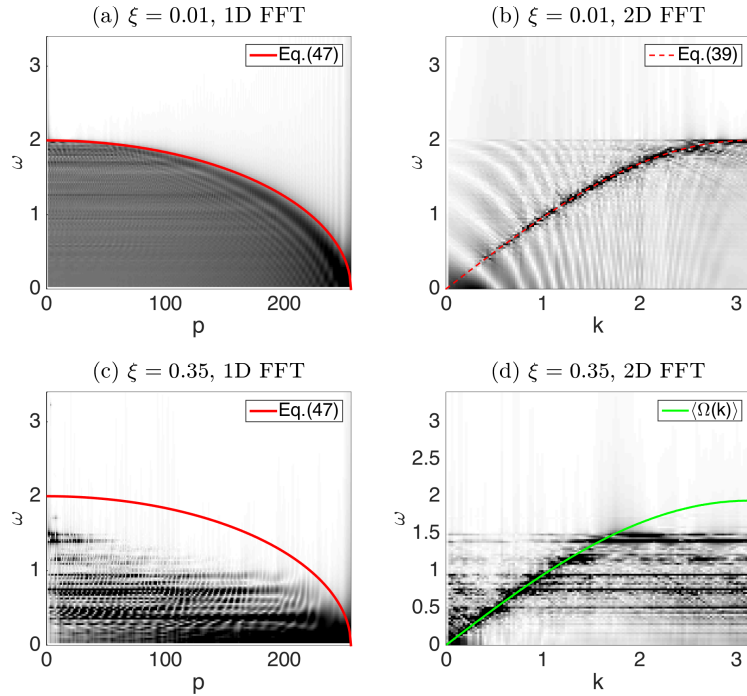
Figure 9. (a) is the temporal Fourier transform of displacement of particles for normal distribution and disorder parameter $\xi = 0.01$ (single realization) with group velocity (v_g) depicting the propagation of wave front and (b) is the temporal as well as spatial Fourier transform (2D FFT, single realization) calculated for obtaining the dispersion relation of a chain, while $\langle \Omega(k) \rangle$ gives the true ensemble averaged (500) dispersion relation from Eq. (43). (c) and (d) are the higher disorder $\xi = 0.35$ counterparts of (a) and (b), respectively.

3.6 Total Energy Dispersion in Disordered Chains

The $\langle \Omega(k) \rangle$ from Eq. (43) which was plotted for $\xi = 0.35$ in Fig. 9(b) is plotted for $\xi = 0.1, 0.2, 0.35, 0.5$ and 0.8 in Fig. 10(a). It is observed that the maximum permissible frequency (Ω_π) above which the waves become evanescent decreases with increasing disorder. The slope of ω v/s k curves indicates the wave speed which clearly can be observed to be decreasing with increasing disorder, confirming what was observed in Sect. 3.4.

3.7 Participation Ratio & Localization length

Figure 11 shows the participation ratio ($\langle P \rangle$), i.e. the localization length ($\langle L \rangle$, from Sect. 2.7) for binned 500 ensemble averaged realizations of chains (with 0.0781 as frequency bin size) and with different disorder parameters ξ. The lowest frequencies have the same localization length $L_{max} = 171$, independent of the disorder of the chain, see Sect. 2.7. Towards higher frequency the localization length decays to zero more rapidly with increasing disorder, characterised by a particular frequency (cross-over or pass frequency) where $p = L_{max}/2$. Unlike infinitely long chains, where $L \propto \omega^{-2}$ (as suggested in Azbel (1983)), the finite
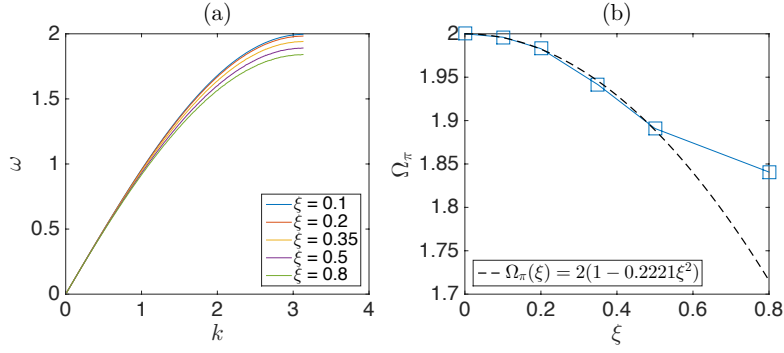
Figure 10. Dispersion relation, $\langle \Omega(k) \rangle$ with respect to different wavenumbers and (b) the maximum permissible frequency for disorder parameters $\xi = 0.0, 0.1, 0.2, 0.35, 0.5$ and 0.8, with empirical quadratic fit given in the inset (ignoring $\xi = 0.8$).
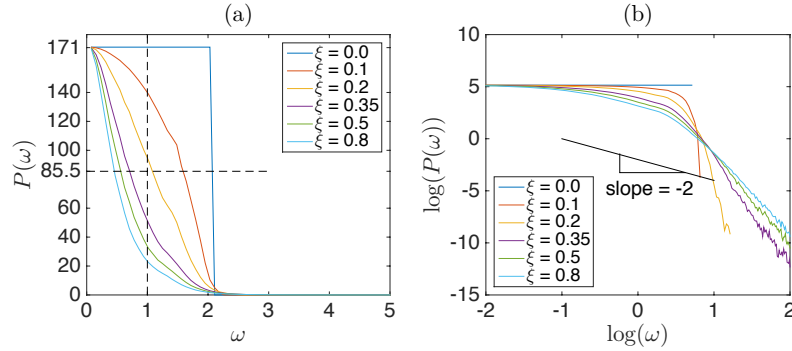
Figure 11. Participation Ratio or localization length with respect to different frequencies for 500 ensembles with $\xi = 0.1, 0.2, 0.35, 0.5$ and 0.8 and bin size = 0.0781.

disordered chains for higher frequencies have $L \propto \omega^{-q}$ where $q \gg 2$, decreasing with increasing disorder. For understanding the effect of disorder on the pass-frequencies (ω_{pass}) associated with the localization length (L), $\omega_{pass(1/2)}$ (the frequency associated with $L_{max}/2$) for different disorder parameters have been plotted in Fig. 12(a) and L associated with $\omega = 1$, scaled with L_{max}, for multiple disorder parameters has been plotted in Fig. 12(b), selected from the dashed line crossings in Fig. 11(a). Both quantities exhibit a decreasing trend with increase in disorder as characterized by the empirical fits:

$$\omega_{pass(1/2)} = \omega_o + (2 - \omega_o)\exp^{-\xi/\xi_\omega} \tag{48}$$

where $\omega_o = 0.3502$ and $\xi_\omega = 0.2536$.

$$L(\omega = 1) = L_o + (L_{max} - L_o)\exp^{-\xi/\xi_L} \tag{49}$$

where $L_o = 2.7668$ and $\xi_L = 0.3165$, with some errors of the order of $\pm 5\%$. Both curves saturate for large ξ values. More data and a closer analysis are necessary for improving this analysis and put a better basis to the fits.
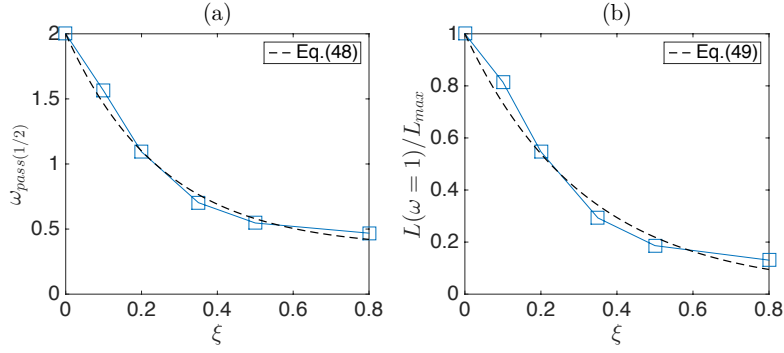
Figure 12. (a) $\omega_{pass(1/2)}$ and (b) Localization length at $\omega = 1$ scaled with maximum localization length (L_{max}) for different ξ.
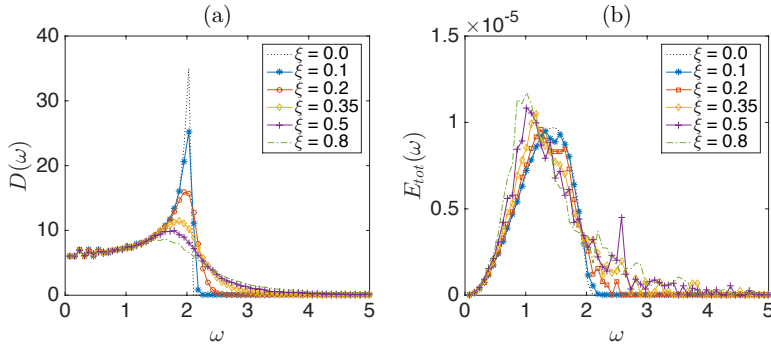
Figure 13. (a) Density of States (DOS) and (b) energies of the binned frequencies for different disorder ξ $\forall$ bin size in ω.

3.8 Total Energy of Eigenmodes

The Density Of States (DOS) or density of vibrational modes is an important quantifying factor in studying the vibrational properties of materials like jammed granular media (Schreck et al. (2014)), etc. However, it tells us only about the number of vibrational modes but, does not paint the complete picture of spectral properties of energy transport. Eq. (A5) gives us the energies of individual eigenmodes and shows that the energy is constant with respect to time. Figure 13(a) plots the ensemble averaged density of states for 500 mass disordered granular chains with frequency bins of size 0.0781. The peak of the density is decreasing with increasing disorder and shifting to smaller ω. Figure 13(b) gives the ensemble averaged energy spectrum for the same frequency bins used in the previous plot (500 realizations) giving an energy distribution over frequency. The shape of the energy distribution is wider over frequency for lower ξ. For larger ξ, the energy distribution becomes more sharp with increasing disorder and shifting to smaller ω. In both plots Fig. 13 (a) and (b), the tails are broader for larger ξ, where the shapes in (a) are independent of driving, while the shapes in (b) depend on the initial condition.

4 Conclusions

An impulse driven wave propagating through a precompressed mass disordered granular chain has been studied. Motivation comes from the existence of force chains which form the backbone network for mechanical wave propagation in granular materials like soil. The scaled standard deviation of the mass probability distribution of the elements/particles of the granular chain has been identified as the relevant disorder parameter (ξ; see Sect. 2.6), as suggested already in Lawney and Luding (2014). Chains with normal, binary and uniform mass distributions have quantitatively identical signal transmission characteristcs as long as the first two moments of the mass distribution are the same and ξ is not too large.

Interestingly, on first sight, the dependence of wave speed on magnitude of disorder looks non-monotonous. This surprising increase of wave-speed for weak disorder, and decrease for stronger disorder, is due to two different effects overlapping: The increase of wave-speed takes place close to the source, see Fig. 7, i.e. our 1D granular chain has the ability to model the physics of accelerating waves, as observed in complex higher dimensional granular structures (Mouraille et al. (2006)). The competing mechanism of decreasing wave-speed with disorder is only clearly observed when the velocities are measured as travel time with maintaining constant separation far away from the source (Fig 8 and Table 6). The group velocity given by Eq. (45) also shows a decrease in wave-speed with increase in disorder. When the travel time is measured from the source, the two mechanisms overlap and interfere, causing the non-monotonous behavior, but possibly allowing for tuning particular propagation characteristics in short chains.

As another main result, Eq. (43) gives an effective, weighted dispersion relation as the normalized first moment of eigen-modal (total) energies with frequency. This gives a much better signal to noise ratio for ω v/s k in comparison to 2D FFT of displacement or velocity signals, reported previously ((Mouraille et al., 2006), O'Donovan et al. (2015)). Figure 10 shows that the upper limit (maximum permissible) frequency due to the discreteness of the system slightly decreases with increasing disorder, ξ, and consistently, waves propagate slightly slower with increasing disorder if scaled by mean mass, i.e. an effect of ξ. From the energy content one also observes (in disordered systems) that waves above a low frequency pass-band (ω_{pass}) become evanescent after they have traversed a localization length, $L = L(\omega)$, associated with a particular pass frequency (ω_{pass}) for which (yet) no analytical prediction is known to the authors (Otsubo et al. (2017)).

The energy analysis presented in this article can be used for understanding pulse propagation in disordered, weakly or strongly non-linear granular chains and its attenuation, widening and acceleration (experimentally and numerically investigated in Langlois and Jia (2015)). It would also be interesting to understand the effect of damping on the eigenmodes, velocity of the propagating wave, changes in frequency filtering and the energy of the eigenmodes. Also, a different kind of averaging (micro-macro transition) should be developed using frequency bands to develop a Master Equation for propagation (or localization) of total energy in terms of wavenumber and frequency at different regimes of disorder, non-linearity, and material properties. Such macro-models, taking into account multiple scattering, dispersion, attenuation, etc. will allow for modeling of realistic wave propagation in granular materials like soil on large scales.

5 Data availability

Data has been generated using the aforementioned theoretical model. The readers can reproduce it by using the equations mentioned in their respective sections.

Appendix A: Total Energy Harmonic Evolution

The Energy of the system (chain) can be calculated by vector multiplications at a particular instance of time, the non-unitary dimension of the vector gives the respective information of the individual particles. The Kinetic Energy of the chain at a particular instant of time is

$$E_{kin}(t) = \frac{1}{2}\mathbf{v}^{\mathrm{T}}\mathbf{Mv} \tag{A1}$$

Starting from the impulse initial condition in Sect. 2.5, using $\mathbf{v} = \mathbf{SC}^{(2)}\mathbf{Ga}$ (Eq. (29) and (30)) and the orthonormality condition $\mathbf{S}^{\mathrm{T}}\mathbf{MS} = \mathbf{I}$ (Eq. (21)), where $\mathbf{I}$ is the identity matrix, the above equation becomes

$$E_{kin}(t) = \frac{1}{2}(\mathbf{SC}^{(2)}\mathbf{Ga})^{\mathrm{T}}\mathbf{M}(\mathbf{SC}^{(2)}\mathbf{Ga})$$
$$= \frac{1}{2}\mathbf{a}^{\mathrm{T}}\mathbf{G}^{\mathrm{T}}(\mathbf{C}^{(2)})^{\mathrm{T}}\mathbf{S}^{\mathrm{T}}\mathbf{MSC}^{(2)}\mathbf{Ga} = \frac{1}{2}\mathbf{a}^{\mathrm{T}}\mathbf{G}\{\mathbf{C}^{(2)}\}^2\mathbf{Ga} = \frac{1}{2}\sum_j a_j^2\omega_j^2\sin^2(\omega_j t) \tag{A2}$$

Since $\mathbf{C}^{(1)}$, $\mathbf{C}^{(2)}$ and $\mathbf{G}$ are diagonal matrices, hence their transposition are equal to their original matrices. Note that there is no summation convention applied here. The Potential Energy of the chain at a particular instant of time is

$$E_{pot}(t) = -\frac{1}{2}\mathbf{u}^{\mathrm{T}}\mathbf{Ku}, \tag{A3}$$

Using $\mathbf{u} = \mathbf{SC}^{(1)}\mathbf{a}$, $\mathbf{v} = \mathbf{SC}^{(2)}\mathbf{Ga}$, Eq. (30), and orthonormality, the above equation can be written as,

$$E_{pot}(t) = -\frac{1}{2}\mathbf{u}^{\mathrm{T}}\mathbf{Ku}$$
$$= -\frac{1}{2}\mathbf{u}^{\mathrm{T}}\mathbf{M}\frac{\mathrm{d}^2\mathbf{u}}{\mathrm{d}t^2}$$
$$= -\frac{1}{2}(\mathbf{SC}^{(1)}\mathbf{a})^{\mathrm{T}}\mathbf{M}\frac{\mathrm{d}\mathbf{v}}{\mathrm{d}t}$$
$$= -\frac{1}{2}(\mathbf{SC}^{(1)}\mathbf{a})^{\mathrm{T}}\mathbf{M}\frac{\mathrm{d}\mathbf{SC}^{(2)}\mathbf{Ga}}{\mathrm{d}t}$$
$$= \frac{1}{2}\mathbf{a}^{\mathrm{T}}\mathbf{C}^{(1)}\mathbf{S}^{\mathrm{T}}\mathbf{MSC}^{(1)}\{\mathbf{G}\}^2\mathbf{a}$$
$$= \frac{1}{2}\mathbf{a}^{\mathrm{T}}\mathbf{G}\{\mathbf{C}^{(1)}\}^2\mathbf{Ga} = \frac{1}{2}\sum_j a_j^2\omega_j^2\cos^2(\omega_j t). \tag{A4}$$

Hence, the Total Energy becomes a sum over all eigenmode energies:

$$E_{tot}(t) = \frac{1}{2}\sum_j a_j^2\omega_j^2, \tag{A5}$$

which is independent of time (the energy of our chain is conserved). This equation (A5) also gives us energy with respect to different eigenmodes of the chain (if we drop the summation). Hence, $E_{tot}(\omega_j) = \frac{1}{2}a_j^2\omega_j^2$. Now, by replacing $\mathbf{u}$, $\mathbf{v}$, $\mathbf{a}$ with their spatial Fourier transform counter parts $\mathcal{U}, \mathcal{V}$ and $\mathcal{A}$ (calligraphic) by using the ansatz in spatial Fourier space as in Eq. (19) for Eq. (18), we obtain the harmonic total energy (in terms of wavenumber):

$$E_{tot}(\omega_j, k) = \frac{1}{2}\mathcal{A}_j^2(k)\omega_j^2. \tag{A6}$$
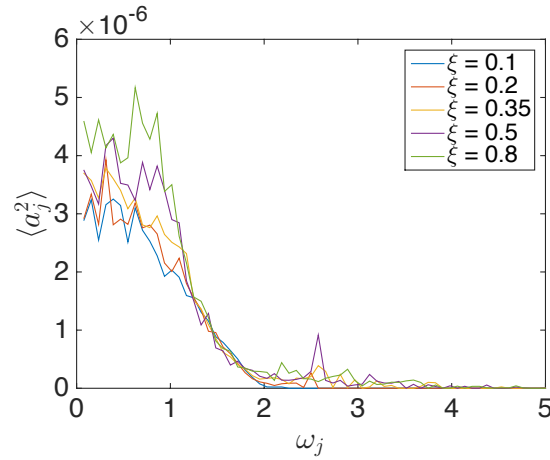
Figure A1. Multiplicative Factor a_j for normal distribution obtained after ensemble averaging (500).

Appendix B: Hertz contact model

If a Hertzian repulsive interaction force is taken into consideration between particles (Landau and Lifshitz (1970), Lawney and Luding (2014))

$$\tilde{\kappa}_{(i,j)} = \tilde{Y}_{(i,j)} \left[\frac{\tilde{r}_i \tilde{r}_j}{\tilde{r}_i + \tilde{r}_j} \right]^{1/2}, \tag{B1}$$

where

$$\tilde{Y}_{(i,j)}^{-1} = \frac{3}{4} \left(\frac{1 - \nu_i^2}{\tilde{E}_i} + \frac{1 - \nu_j^2}{\tilde{E}_j} \right). \tag{B2}$$

$\tilde{E}_i$ and ν_i are the elastic modulus and Poisson's ratio, respectively, of particle i. If the particles are made up of the same material, $\tilde{Y}_{(i,j)}$ and ν become same for all the contacts,

$$\tilde{Y}^{-1} = \frac{3}{2} \left(\frac{1 - \nu^2}{\tilde{E}} \right). \tag{B3}$$

The characteristic stiffness of the contact is

$$\tilde{\kappa}_o = \frac{\tilde{E}}{1 - \nu^2} \left[\frac{2\tilde{m}_o}{243\pi\tilde{\rho}} \right]^{1/6}. \tag{B4}$$

The characteristic initial overlap becomes

$$\tilde{\Delta}_o = \left(\frac{\tilde{F}_o}{\tilde{\kappa}_o} \right)^{2/3}. \tag{B5}$$

The characteristic time is

$$\tilde{t}_c = \frac{1}{\tilde{\Delta}_o^{1/4}} \sqrt{\frac{1 - \nu^2}{\tilde{E}}} \left[\frac{243\pi\tilde{\rho}\tilde{m}_o^5}{2} \right]^{1/12}. \tag{B6}$$

The scaled stiffness ratio is

$$\kappa_{(i,j)} = \frac{\tilde{\kappa}_{(i,j)}}{\tilde{\kappa}_o} = \sqrt{\frac{2}{b^{(i)1/3} + b^{(j)1/3}}} \left(b^{(i)} b^{(j)}\right)^{1/6}. \tag{B7}$$

The initial overlap during static equilibrium can be formulated as

$$\Delta_{(i,j)} = \frac{\tilde{\Delta}_{(i,j)}}{\tilde{\Delta}_o} = \kappa_{(i,j)}^{-2/3}. \tag{B8}$$

5 Appendix C: Matching the first two moments of different distributions (normal, uniform and binary).

The raw n^{th} moment of a probability distribution $f^{(q)}(\tilde{m})$ is defined as

$$\tilde{M}_n^{(q)} = \int_{-\infty}^{\infty} \tilde{m}^n f^{(q)}(\tilde{m}) \mathrm{d}\tilde{m}, \tag{C1}$$

where, $f^{(q)}(\tilde{m})$ is the distribution, q is the type of distribution and $\tilde{m}$ is the variable for which the distribution has been defined. q is n for normal distribution, u for uniform distribution and bi for binary distribution. The scaled moment is defined as

$$
\begin{aligned}
M_n^{(q)} &= \frac{\tilde{M}_n^{(q)}}{(\tilde{M}_1^{(q)})^n}, \\
&= \frac{\int_{-\infty}^{\infty} \tilde{m}^n f(\tilde{m}) \mathrm{d}\tilde{m}}{(\int_{-\infty}^{\infty} \tilde{m} f(\tilde{m}) \mathrm{d}\tilde{m})^n} = \frac{\int_{-\infty}^{\infty} \tilde{m}^n f(\tilde{m}) \mathrm{d}\tilde{m}}{(\tilde{M}_1)^n}, \text{ (where first raw moment is the average of the distribution}(\tilde{M}_1)) \\
&= \int_{-\infty}^{\infty} \left(\frac{\tilde{m}}{\tilde{M}_1}\right)^n f(\tilde{m}) \mathrm{d}\tilde{m} = \int_{-\infty}^{\infty} b^n \{\tilde{M}_1 f(\tilde{m})\} \mathrm{d}b, \text{ where } b = \tilde{m}/\tilde{M}_1 \text{ is the scaled mass (Sect. 2.1)} \\
&= \int_{-\infty}^{\infty} b^n f(b) \mathrm{d}b, \text{ with } f(b) \text{ as the scaled mass distribution} \tag{C2}
\end{aligned}
$$

In case of particle mass distributions, only positive values can be considered so that the lower limit is to be replaced by zero, which has consequences for larger ξ.

C1 Normal Distribution

The unscaled normal distribution is given as

$$f^{(n)}(\tilde{m}) = \frac{1}{\tilde{\xi}^{(n)}\sqrt{2\pi}} e^{-\frac{(\tilde{m}-\tilde{M}_1)^2}{2(\tilde{\xi}^{(n)})^2}}, \tag{C3}$$

where, $\tilde{\xi}^{(n)}$ is the standard deviation and $\tilde{M}_1$ is the average of the distribution. The scaled normal distribution is given as

$$f^{(n)}(b) = \tilde{M}_1 f^{(n)}(\tilde{m}) = \frac{1}{\xi^{(n)}\sqrt{2\pi}} e^{-\frac{(b-1)^2}{2(\xi^{(n)})^2}}. \tag{C4}$$

where $b = \tilde{m}/\tilde{M}_1$ is the scaled mass and $\xi^{(n)} = \tilde{\xi}^{(n)}/\tilde{M}_1$ is the scaled standard deviation which is the disorder parameter for the one dimensional chain.

C1.1 First Moment

The first scaled moment of the normal distribution is given as

$$M_1^{(n)} = \int\limits_{-\infty}^{\infty} b \frac{1}{\xi^{(n)}\sqrt{2\pi}} e^{-\frac{(b-1)^2}{2(\xi^{(n)})^2}} \, \mathrm{d}b, = \underbrace{\int\limits_{-\infty}^{\infty} (b-1) \frac{1}{\xi^{(n)}\sqrt{2\pi}} e^{-\frac{(b-1)^2}{2(\xi^{(n)})^2}} \, \mathrm{d}b}_{\text{non-even power of } b} + \underbrace{\int\limits_{-\infty}^{\infty} \frac{1}{\xi^{(n)}\sqrt{2\pi}} e^{-\frac{(b-1)^2}{2(\xi^{(n)})^2}} \, \mathrm{d}b}_{\text{even power of } b},$$

$$= 0 + \frac{1}{\sqrt{\pi}} \times \sqrt{\pi} = 1. \tag{C5}$$

Hence, the first scaled moment of the normal distribution is 1.

5 C1.2 Second Moment

The Gaussian integral (normalizing condition) can be used, differentiated with respect to $(\xi^{(n)})^2$ to get

$$-\frac{1}{2(\xi^{(n)})^2 \sqrt{2\pi(\xi^{(n)})^2}} \int\limits_{-\infty}^{\infty} e^{-\frac{(b-1)^2}{2(\xi^{(n)})^2}} \, \mathrm{d}b + \frac{1}{\sqrt{2\pi(\xi^{(n)})^2}} \int\limits_{-\infty}^{\infty} \frac{(b-1)^2}{2(\xi^{(n)})^4} e^{-\frac{(b-1)^2}{2(\xi^{(n)})^2}} \, \mathrm{d}b = 0,$$

Multiplication by $2(\xi^{(n)})^4$ yields

$$\Rightarrow \frac{1}{\sqrt{(\xi^{(n)})^2 2\pi}} \int\limits_{-\infty}^{\infty} (b-1)^2 e^{-\frac{(b-1)^2}{2(\xi^{(n)})^2}} \, \mathrm{d}b = \frac{(\xi^{(n)})^2}{\sqrt{2\pi(\xi^{(n)})^2}} \underbrace{\int\limits_{-\infty}^{\infty} e^{-\frac{(b-1)^2}{2(\xi^{(n)})^2}} \, \mathrm{d}b}_{\text{Normalizing condition} = 1},$$

$$\Rightarrow M_2^{(n)} = 1 + (\xi^{(n)})^2. \tag{C6}$$

Taking $\xi^{(n)} = \xi$, the second scaled moment of the normal distribution is $1 + \xi^2$.

C2 Binary Distribution

10 The unscaled binary distribution is given by

$$f^{(bi)}(\tilde{m}) = \frac{\delta(\tilde{m} - (\tilde{M}_1 + \tilde{\xi}^{(bi)}))}{2} + \frac{\delta(\tilde{m} - (\tilde{M}_1 - \tilde{\xi}^{(bi)}))}{2}, \tag{C7}$$

with the Kronecker $\delta(0) = 1$ and the scaled binary distribution is given as

$$f^{(bi)}(b) = \tilde{M}_1 f^{(bi)}(\tilde{m}),$$
$$= \frac{\delta\{b - (1 - \xi^{(bi)})\} + \delta\{b - (1 + \xi^{(bi)})\}}{2} \tag{C8}$$

where $b = \tilde{m}/\tilde{M}_1$ is the scaled mass and $\xi^{(bi)} = \tilde{\xi}^{(bi)}/\tilde{M}_1$ is the scaled standard deviation, which is the disorder parameter for

15 the one dimensional chain.

C2.1 First Moment

The first scaled moment of the distribution is given as

$$M_1^{(bi)} = \int_{-\infty}^{\infty} b f^{(bi)}(b) \mathrm{d}b = \frac{1 - \xi^{(bi)}}{2} + \frac{1 + \xi^{(bi)}}{2} = 1. \tag{C9}$$

Hence, the first scaled moment of the binary distribution is 1.

C2.2 Second Moment

The second scaled moment of the binary distribution is given as follows :

$$M_2^{(bi)} = \int_{-\infty}^{\infty} b^2 f^{(bi)}(b) \mathrm{d}b = \frac{(1 - \xi^{(bi)})^2}{2} + \frac{(1 + \xi^{(bi)})^2}{2} = 1 + (\xi^{(bi)})^2. \tag{C10}$$

Taking $\xi^{(n)} = \xi^{(bi)} = \xi$, the second scaled moment of the binary distribution is $1 + \xi^2$.

C3 Uniform Distribution

The unscaled uniform distribution for the mass distribution is given by

$$f^{(u)}(\tilde{m}) = \begin{cases} \frac{1}{2\tilde{\xi}^{(u)}} & \text{for } \tilde{M}_1 - \tilde{\xi}^{(u)} \le \tilde{m} \le \tilde{M}_1 + \tilde{\xi}^{(u)} \\ 0 & \text{for } \tilde{m} < \tilde{M}_1 - \tilde{\xi}^{(u)} \text{ or } \tilde{m} > \tilde{M}_1 + \tilde{\xi}^{(u)} \end{cases} \tag{C11}$$

The value of the mass is $\frac{1}{2\tilde{\xi}^{(u)}}$ in the interval $\left[\tilde{M}_1 - \tilde{\xi}^{(u)}, \tilde{M}_1 + \tilde{\xi}^{(u)} \right]$ and 0 elsewhere. The scaled uniform distribution is given as

$$f^{(u)}(b) = \tilde{M}_1 f^{(u)}(\tilde{m}),$$

$$= \begin{cases} \frac{1}{2\xi^{(u)}} & \text{for } 1 - \xi^{(u)} \le b \le 1 + \xi^{(u)} \\ 0 & \text{for } b < 1 - \xi^{(u)} \text{ or } b > 1 + \xi^{(u)} \end{cases} \tag{C12}$$

The scaled masses (b) are selected from the interval $[1 - \xi, 1 + \xi]$ to approximately p-reserve symmetry about the scaled mean.

C3.1 First Moment

The first scaled moment of the distribution is given as

$$M_1^{(u)} = \int_{-\infty}^{\infty} b f^{(u)}(b) \mathrm{d}b = \int_{1-\xi^{(u)}}^{1+\xi^{(u)}} \frac{b}{2\xi^{(u)}} \mathrm{d}b = \frac{b^2}{4\xi^{(u)}} \Bigg|_{1-\xi^{(u)}}^{1+\xi^{(u)}} = 1. \tag{C13}$$

Hence, the first scaled moment of the uniform distribution is 1.

C3.2 Second Moment

The second moment of the distribution is given as

$$M_2^{(u)} = \int\limits_{-\infty}^{\infty} b^2 f^{(u)}(b)\mathrm{d}b = \int\limits_{1-\xi^{(u)}}^{1+\xi^{(u)}} \frac{b^2}{2\xi}\mathrm{d}b = \frac{b^3}{6\xi^{(u)}}\bigg|_{1-\xi^{(u)}}^{1+\xi^{(u)}} = 1 + \frac{(\xi^{(u)})^2}{3} \tag{C14}$$

Taking $\xi^{(u)} = \sqrt{3}\xi^{(n)} = \sqrt{3}\xi^{(bi)} = \sqrt{3}\xi$ and using Eq. (C14) yields

$$M_2^{(u)} = 1 + \frac{(\xi^{(u)})^2}{3} = 1 + \xi^2, \tag{C15}$$

thereby, placing a limit on the uniform distribution ($[1 - \sqrt{3}\xi, 1 + \sqrt{3}\xi]$) so that the first two moments of three distributions are identical except for large ξ.

From equations (C4), (C9) and (C13), it can be said that the first moment of the distributions have been matched. From equations (C6), (C10) and after a placing a limit on the uniform distribution. Equation (C15) shows that the second moments of the distributions are matched. However, for large disorder, there is a need for correction as $b > 0$ cannot be negative.

Author contributions. The manuscript was prepared by R. Shrivastava and was co-authored by S. Luding.

Acknowledgements. This work is part of the Industrial Partnership Programme (IPP) 'Computational sciences for energy research' of the Foundation for Fundamental Research on Matter (FOM), which is part of the Netherlands Organisation for Scientific Research (NWO). This research programme is co-financed by Shell Global Solutions International B.V.

References

Achilleos, V., Theocharis, G., and Skokos, C.: Energy transport in one-dimensional disordered granular solids, Phys. Rev. E, 93, 022 903, doi:10.1103/PhysRevE.93.022903, http://link.aps.org/doi/10.1103/PhysRevE.93.022903, 2016.

Aki, K. and Richards, P.: Quantitative Seismology, Geology (University Science Books).: Seismology, University Science Books, https://books.google.nl/books?id=sRhawFG5_EcC, 2002.

Allen, P. B. and Kelner, J.: Evolution of a vibrational wave packet on a disordered chain, American Journal of Physics, 66, 1998.

Anderson, P. W.: Absence of Diffusion in Certain Random Lattices, Phys. Rev., 109, 1492–1505, doi:10.1103/PhysRev.109.1492, http://link.aps.org/doi/10.1103/PhysRev.109.1492, 1958.

Azbel, M. Y.: One dimension. Thermodynamics, kinetics, eigenstates, and universality, Phys. Rev. B, 27, 3901–3904, doi:10.1103/PhysRevB.27.3901, http://link.aps.org/doi/10.1103/PhysRevB.27.3901, 1983.

Bell, R. J. and Dean, P.: Atomic vibrations in vitreous silica, Discuss. Faraday Soc., 50, 55–61, doi:10.1039/DF9705000055, http://dx.doi.org/10.1039/DF9705000055, 1970.

Boechler, N., Theocharis, G., and Daraio, C.: Bifurcation-based acoustic switching and rectification, Nat Mater, 10, 665–668, http://dx.doi.org/10.1038/nmat3072, 2011.

Brillouin, L.: Wave propagation in periodic structures, Dover Phoenix Editions, McGraw-Hill Book Company, Inc., https://books.google.nl/books?id=m2WmGiU5nUwC&printsec=frontcover&dq=Wave+propagation+in+periodic+structures+citation&hl=en&sa=X&ei=OobYVN2DEc_tavn4gagO&ved=0CCAQ6AEwAA#v=onepage&q=Wave%20propagation%20in%20periodic%20structures%20citation&f=false, 1946.

Coste, C. and Gilles, B.: Sound propagation in a constrained lattice of beads: High-frequency behavior and dispersion relation, Phys. Rev. E, 77, 021 302, doi:10.1103/PhysRevE.77.021302, http://link.aps.org/doi/10.1103/PhysRevE.77.021302, 2008.

Daraio, C., Nesterenko, V. F., Herbold, E. B., and Jin, S.: Energy Trapping and Shock Disintegration in a Composite Granular Medium, Phys. Rev. Lett., 96, 058 002, doi:10.1103/PhysRevLett.96.058002, http://link.aps.org/doi/10.1103/PhysRevLett.96.058002, 2006.

Dyskin, A. V., Pasternak, E., and Pelinovsky, E.: Periodic motions and resonances of impact oscillators, Journal of Sound and Vibration, 331, 2856 – 2873, doi:https://doi.org/10.1016/j.jsv.2012.01.031, http://www.sciencedirect.com/science/article/pii/S0022460X12001010, 2012.

Dyskin, A. V., Pasternak, E., and Shufrin, I.: Structure of resonances and formation of stationary points in symmetrical chains of bilinear oscillators, Journal of Sound and Vibration, 333, 6590 – 6606, doi:https://doi.org/10.1016/j.jsv.2014.06.044, http://www.sciencedirect.com/science/article/pii/S0022460X14005513, 2014.

Esin, M., Pasternak, E., and Dyskin, A. V.: Stability of 2D discrete mass-spring systems with negative stiffness springs, physica status solidi (b), 253, 1395–1409, doi:10.1002/pssb.201552763, http://dx.doi.org/10.1002/pssb.201552763, 2016.

Gilles, B. and Coste, C.: Low-Frequency Behavior of Beads Constrained on a Lattice, Phys. Rev. Lett., 90, 174 302, doi:10.1103/PhysRevLett.90.174302, http://link.aps.org/doi/10.1103/PhysRevLett.90.174302, 2003.

Güven, I.: Hydraulical and acoustical properties of porous sintered glass bead systems: experiments, theory, & simulations, Ph.D. thesis, Enschede, http://doc.utwente.nl/100546/, 2016.

Guzek, A., Dyskin, A. V., Pasternak, E., and Shufrin, I.: Asymptotic analysis of bilinear oscillators with preload, International Journal of Engineering Science, 106, 125 – 141, doi:https://doi.org/10.1016/j.ijengsci.2016.05.006, http://www.sciencedirect.com/science/article/pii/S0020722516300738, 2016.

Jia, X.: Codalike Multiple Scattering of Elastic Waves in Dense Granular Media, Phys. Rev. Lett., 93, 154 303, doi:10.1103/PhysRevLett.93.154303, http://link.aps.org/doi/10.1103/PhysRevLett.93.154303, 2004.

Jia, X., Caroli, C., and Velicky, B.: Ultrasound Propagation in Externally Stressed Granular Media, Phys. Rev. Lett., 82, 1863–1866, doi:10.1103/PhysRevLett.82.1863, http://link.aps.org/doi/10.1103/PhysRevLett.82.1863, 1999.

5   Landau, L. D. and Lifshitz, E. M.: Theory of elasticity, Pergamon Press, 1970.

Langlois, V. and Jia, X.: Sound pulse broadening in stressed granular media, Phys. Rev. E, 91, 022 205, doi:10.1103/PhysRevE.91.022205, http://link.aps.org/doi/10.1103/PhysRevE.91.022205, 2015.

Larose, E., Margerin, L., van Tiggelen, B. A., and Campillo, M.: Weak Localization of Seismic Waves, Phys. Rev. Lett., 93, 048 501, doi:10.1103/PhysRevLett.93.048501, http://link.aps.org/doi/10.1103/PhysRevLett.93.048501, 2004.

10 Lawney, B. and Luding, S.: Frequency filtering in disordered granular chains, Acta Mechanica, 225, 2385–2407, doi:10.1007/s00707-014-1130-4, http://dx.doi.org/10.1007/s00707-014-1130-4, 2014.

Lawney, B. P. and Luding, S.: Mass–disorder effects on the frequency filtering in one–dimensional discrete particle systems, AIP Conference Proceedings, 1542, 535–538, doi:http://dx.doi.org/10.1063/1.4811986, http://scitation.aip.org/content/aip/proceeding/aipcp/10.1063/1.4811986, 2013.

15 Luding, S. and Mouraille, O.: Mechanic waves in sand: effect of polydispersity, in: PARTEC 2007, Congress on Particle Technology, edited by Peukert, W. and Schreglmann, C., University of Erlangen-Nuremberg, Institute of Particle Technology, http://doc.utwente.nl/80328/, 2008.

Makse, H. A., Gland, N., Johnson, D. L., and Schwartz, L.: Granular packings: Nonlinear elasticity, sound propagation, and collective relaxation dynamics, Phys. Rev. E, 70, 061 302, doi:10.1103/PhysRevE.70.061302, http://link.aps.org/doi/10.1103/PhysRevE.70.061302, 20   2004.

Marketos, G. and O'Sullivan, C.: A micromechanics-based analytical method for wave propagation through a granular material, Soil Dynamics and Earthquake Engineering, 45, 25 – 34, doi:http://dx.doi.org/10.1016/j.soildyn.2012.10.003, http://www.sciencedirect.com/science/article/pii/S0267726112002382, 2013.

Matsuyama, K. and Katsuragi, H.: Power law statistics of force and acoustic emission from a slowly penetrated granular bed, Nonlinear 25 Processes in Geophysics, 21, 1–8, doi:10.5194/npg-21-1-2014, http://www.nonlin-processes-geophys.net/21/1/2014/, 2014.

Merkel, A., Tournat, V., and Gusev, V.: Dispersion of elastic waves in three-dimensional noncohesive granular phononic crystals: Properties of rotational modes, Phys. Rev. E, 82, 031 305, doi:10.1103/PhysRevE.82.031305, http://link.aps.org/doi/10.1103/PhysRevE.82.031305, 2010.

Mouraille, O.: Sound propagation in dry granular materials : discrete element simulations, theory, and experiments, Ph.D. thesis, Enschede, 30 the Netherlands, http://doc.utwente.nl/60697/, 2009.

Mouraille, O. and Luding, S.: Sound wave propagation in weakly polydisperse granular materials, Ultrasonics, 48, 498 – 505, doi:http://dx.doi.org/10.1016/j.ultras.2008.03.009, http://www.sciencedirect.com/science/article/pii/S0041624X08000462, selected Papers from {ICU} 2007, 2008.

Mouraille, O., Mulder, W. A., and Luding, S.: Sound wave acceleration in granular materials, Journal of Statistical Mechanics: Theory and 35 Experiment, 2006, P07 023, http://stacks.iop.org/1742-5468/2006/i=07/a=P07023, 2006.

Nesterenko, V.: Propagation of nonlinear compression pulses in granular media, J. Appl. Mech. Tech. Phys., 24, 733–743, 1983.

O'Donovan, J., O'Sullivan, C., Marketos, G., and Muir Wood, D.: Analysis of bender element test interpretation using the discrete element method, Granular Matter, 17, 197–216, doi:10.1007/s10035-015-0552-6, http://dx.doi.org/10.1007/s10035-015-0552-6, 2015.

O'Donovan, J., Ibraim, E., O'Sullivan, C., Hamlin, S., Muir Wood, D., and Marketos, G.: Micromechanics of seismic wave propagation in granular materials, Granular Matter, 18, 56, doi:10.1007/s10035-015-0599-4, http://dx.doi.org/10.1007/s10035-015-0599-4, 2016.

Ogarko, V. and Luding, S.: Prediction of polydisperse hard-sphere mixture behavior using tridisperse systems, Soft Matter, 9, 9530–9534, doi:10.1039/C3SM50964H, http://dx.doi.org/10.1039/C3SM50964H, 2013.

5 Ostojic, S., Somfai, E., and Nienhuis, B.: Scale invariance and universality of force networks in static granular matter, Nature, 439, 828–830, http://dx.doi.org/10.1038/nature04549, 2006.

Otsubo, M., O'Sullivan, C., Hanley, K., and Sim, W.: Influence of packing density and stress on the dynamic response of granular materials, Granular Matter, 2017.

Owens, E. T. and Daniels, K. E.: Sound propagation and force chains in granular materials, EPL (Europhysics Letters), 94, 54 005, http:
10 //stacks.iop.org/0295-5075/94/i=5/a=54005, 2011.

Pasternak, E. and Mühlhaus, H.-B.: Generalised homogenisation procedures for granular materials, Journal of Engineering Mathematics, 52, 199–229, doi:10.1007/s10665-004-3950-z, http://dx.doi.org/10.1007/s10665-004-3950-z, 2005.

Pasternak, E., Dyskin, A. V., and Sevel, G.: Chains of oscillators with negative stiffness elements, Journal of Sound and Vibration, 333, 6676 – 6687, doi:https://doi.org/10.1016/j.jsv.2014.06.045, http://www.sciencedirect.com/science/article/pii/S0022460X14005525, 2014.

15 Pasternak, E., Dyskin, A. V., Esin, M., Hassan, G. M., and MacNish, C.: Rotations and pattern formation in granular materials under loading, Philosophical Magazine, 95, 3122–3145, doi:10.1080/14786435.2015.1059517, http://dx.doi.org/10.1080/14786435.2015.1059517, 2015.

Sato, H.: Seismic Waves in Heterogeneous Earth, Scattering of, pp. 788–804, Springer New York, New York, NY, doi:10.1007/978-1-4419-7695-6_42, http://dx.doi.org/10.1007/978-1-4419-7695-6_42, 2011.

20 Scales, J. A. and Van Vleck, E. S.: Lyapunov Exponents and Localization in Randomly Layered Media, J. Comput. Phys., 133, 27–42, doi:10.1006/jcph.1997.5643, http://dx.doi.org/10.1006/jcph.1997.5643, 1997.

Schreck, C. F., O'Hern, C. S., and Shattuck, M. D.: Vibrations of jammed disk packings with Hertzian interactions, Granular Matter, 16, 209–216, doi:10.1007/s10035-013-0458-0, http://dx.doi.org/10.1007/s10035-013-0458-0, 2014.

Sheng, P.: Introduction to Wave Scattering, Localization and Mesoscopic Phenomena; 2nd ed., Springer, Dordrecht, https://cds.cern.ch/
25 record/1250571, 2006.

Snieder, R., Grêt, A., Douma, H., and Scales, J.: Coda Wave Interferometry for Estimating Nonlinear Behavior in Seismic Velocity, Science, 295, 2253–2255, doi:10.1126/science.1070015, http://science.sciencemag.org/content/295/5563/2253, 2002.

Somfai, E., Roux, J.-N., Snoeijer, J. H., van Hecke, M., and van Saarloos, W.: Elastic wave propagation in confined granular systems, Phys. Rev. E, 72, 021 301, doi:10.1103/PhysRevE.72.021301, http://link.aps.org/doi/10.1103/PhysRevE.72.021301, 2005.

30 Tournat, V. and Gusev, V.: Acoustics of unconsolidated "model" granular media: An overview of recent results and several open problems, Acta Acustica united with Acustica, 96, 208–224, 2010.

Tournat, V., Gusev, V. E., and Castagnède, B.: Self-demodulation of elastic waves in a one-dimensional granular chain, Phys. Rev. E, 70, 056 603, doi:10.1103/PhysRevE.70.056603, http://link.aps.org/doi/10.1103/PhysRevE.70.056603, 2004.

Upadhyaya, N., Gómez, L. R., and Vitelli, V.: Soliton Attenuation and Emergent Hydrodynamics in Fragile Matter, Phys. Rev. X, 4, 011 045,
35 doi:10.1103/PhysRevX.4.011045, http://link.aps.org/doi/10.1103/PhysRevX.4.011045, 2014.

van den Wildenberg, S., van Hecke, M., and Jia, X.: Evolution of granular packings by nonlinear acoustic waves, EPL (Europhysics Letters), 101, 14 004, http://stacks.iop.org/0295-5075/101/i=1/a=14004, 2013.

Van Der Baan, M.: Acoustic wave propagation in one dimensional random media: the wave localization approach, Geophysical Journal International, 145, 631–646, doi:10.1046/j.1365-246x.2001.01405.x, http://gji.oxfordjournals.org/content/145/3/631.abstract, 2001.

Weaver, R. L.: Information from Seismic Noise, Science, 307, 1568–1569, doi:10.1126/science.1109834, http://science.sciencemag.org/content/307/5715/1568, 2005.

5   Yang, J. and Sutton, M.: Nonlinear wave propagation in a hexagonally packed granular channel under rotational dynamics, International Journal of Solids and Structures, 77, 65 – 73, doi:http://dx.doi.org/10.1016/j.ijsolstr.2015.07.017, http://www.sciencedirect.com/science/article/pii/S0020768315003236, 2015.

Zeravcic, Z., Xu, N., Liu, A. J., Nagel, S. R., and van Saarloos, W.: Excitations of ellipsoid packings near jamming, EPL (Europhysics Letters), 87, 26 001, http://stacks.iop.org/0295-5075/87/i=2/a=26001, 2009.

Table 1. Scaled Moments of ensemble averaged distributions (500 ensembles) used for the one-dimensional chain (256 element long).

Distribution	Disorder	$< M_1 >$	$< M_2 >$	$< M_3 >$	$< M_4 >$	$< M_5 >$	Ξ	Ξ^2
Normal Distribution	$\xi = 0.0$	1.0000	1.0000	1.0000	1.0000	1.0000	0.0000	0.0000
	$\xi = 0.1$	1.0000	1.0099	1.0298	1.0600	1.1010	0.1	0.0100
	$\xi = 0.2$	1.0000	1.0398	1.1194	1.2436	1.4219	0.1999	0.0400
	$\xi = 0.35$	1.0000	1.1190	1.3590	1.7630	2.4184	0.3462	0.1195
	$\xi = 0.5$	1.0000	1.2053	1.6366	2.4335	3.8973	0.4661	0.2061
	$\xi = 0.8$	1.0000	1.3055	2.0104	3.5037	6.7333	0.6415	0.3067
Binary Distribution	$\xi = 0.0$	1.0000	1.0000	1.0000	1.0000	1.0000	0.0000	0.0000
	$\xi = 0.1$	1.0000	1.0100	1.0299	1.0599	1.1001	0.1000	0.0100
	$\xi = 0.2$	1.0000	1.0398	1.1196	1.2408	1.4068	0.2000	0.0400
	$\xi = 0.35$	1.0000	1.1221	1.3666	1.7489	2.2998	0.3501	0.1226
	$\xi = 0.5$	1.0000	1.2495	1.7497	2.5653	3.8255	0.5002	0.2505
	$\xi = 0.8$	1.0000	1.6413	2.9323	5.3034	9.6263	0.8014	0.6438
Uniform Distribution	$\xi = 0.0$	1.0000	1.0000	1.0000	1.0000	1.0000	0.0000	0.0000
	$\xi = 0.1$	1.0000	1.0100	1.0300	1.0602	1.1009	0.1002	0.0100
	$\xi = 0.2$	1.0000	1.0400	1.1201	1.2431	1.4148	0.2004	0.0402
	$\xi = 0.35$	1.0000	1.1227	1.3682	1.7639	2.3646	0.3508	0.1232
	$\xi = 0.5$	1.0000	1.2508	1.7529	2.6212	4.0859	0.5011	0.2517
	$\xi = 0.8$	$---$	$---$	$---$	$---$	$---$	$---$	$---$

Table 2. Unscaled Moments of ensemble averaged distributions (500 ensembles) used for the one-dimensional chain (256 element long).

Distribution	Disorder	$< \tilde{M}_1 >$	$< \tilde{M}_2 >$	$< \tilde{M}_3 >$	$< \tilde{M}_4 >$	$< \tilde{M}_5 >$	$\tilde{\Xi}$	$\tilde{\Xi}^2$
Normal Distribution	$\xi = 0.0$	1.0000	1.0000	1.0000	1.0000	1.0000	0.0000	0.0000
	$\xi = 0.1$	1.0000	1.0100	1.0299	1.0601	1.1013	0.0999	0.0100
	$\xi = 0.2$	1.0000	1.0399	1.1197	1.2443	1.4232	0.1999	0.0400
	$\xi = 0.35$	1.0022	1.1242	1.3689	1.7807	2.4492	0.3462	0.1195
	$\xi = 0.5$	1.0274	1.2728	1.7768	2.7163	4.4725	0.4661	0.2061
	$\xi = 0.8$	1.1581	1.7540	3.1363	6.3458	14.1470	0.6415	0.3067
Binary Distribution	$\xi = 0.0$	1.0000	1.0000	1.0000	1.0000	1.0000	0.0000	0.0000
	$\xi = 0.1$	1.0001	1.0102	1.0303	1.0605	1.1010	0.1000	0.0100
	$\xi = 0.2$	1.0002	1.0404	1.1206	1.2424	1.4091	0.2000	0.0400
	$\xi = 0.35$	1.0003	1.1232	1.3686	1.7516	2.3022	0.3500	0.1225
	$\xi = 0.5$	1.0005	1.2510	1.7516	2.5650	3.8162	0.5000	0.2500
	$\xi = 0.8$	1.0008	1.6416	2.9229	5.2548	9.4573	0.8000	0.6400
Uniform Distribution	$\xi = 0.0$	1.0000	1.0000	1.0000	1.0000	1.0000	0.0000	0.0000
	$\xi = 0.1$	1.0001	1.0102	1.0304	1.0608	1.1017	0.1002	0.0100
	$\xi = 0.2$	1.0001	1.0405	1.1210	1.2446	1.4170	0.2004	0.0400
	$\xi = 0.35$	1.0003	1.1236	1.3699	1.7665	2.3674	0.3508	0.1232
	$\xi = 0.5$	1.0004	1.2519	1.7545	2.6211	4.0781	0.5011	0.2517
	$\xi = 0.8$	– – –	– – –	– – –	– – –	– – –	– – –	– – –

Table 3. Moments of ensemble averaged distributions (10000 ensembles) used for the one-dimensional chain (256 element long).

Distribution	Disorder	$< M_1 >$	$< M_2 >$	$< M_3 >$	$< M_4 >$	$< M_5 >$	Ξ	Ξ^2
	$\xi = 0.0$	1.0000	1.0000	1.0000	1.0000	1.0000	0.0000	0.0000
	$\xi = 0.1$	1.0000	1.0100	1.0299	1.0601	1.1011	0.0999	0.0100
Normal	$\xi = 0.2$	1.0000	1.0399	1.1196	1.2439	1.4225	0.1998	0.04
Distribution	$\xi = 0.35$	1.0000	1.1192	1.3598	1.7648	2.4222	0.3456	0.1197
	$\xi = 0.5$	1.0000	1.2093	1.6491	2.4617	3.9545	0.4579	0.2101
	$\xi = 0.8$	1.0000	1.3319	2.0893	3.6833	7.1170	0.5767	0.3332
	$\xi = 0.0$	1.0000	1.0000	1.0000	1.0000	1.0000	0.0000	0.0000
	$\xi = 0.1$	1.0000	1.0100	1.0299	1.0599	1.1001	0.1000	0.0100
Binary	$\xi = 0.2$	1.0000	1.0399	1.1196	1.2409	1.4069	0.2000	0.0400
Distribution	$\xi = 0.35$	1.0000	1.1222	1.3668	1.7494	2.3006	0.3501	0.1226
	$\xi = 0.5$	1.0000	1.2496	1.7502	2.5665	3.8279	0.5004	0.2506
	$\xi = 0.8$	1.0000	1.6417	2.9340	5.3080	9.6373	0.8017	0.6442
	$\xi = 0.0$	1.0000	1.0000	1.0000	1.0000	1.0000	0.0000	0.0000
	$\xi = 0.1$	1.0000	1.0100	1.0299	1.0600	1.1006	0.1000	0.0100
Uniform	$\xi = 0.2$	1.0000	1.0399	1.1197	1.2422	1.4134	0.2000	0.0400
Distribution	$\xi = 0.35$	1.0000	1.1223	1.3670	1.7616	2.3605	0.3501	0.1227
	$\xi = 0.5$	1.0000	1.2499	1.7507	2.6167	4.0775	0.5005	0.2509
	$\xi = 0.8$	− − −	− − −	− − −	− − −	− − −	− − −	− − −

Table 4. Scaled Coherent Wave Velocity Picking for different particles before and after localization length for a disordered chain with normal distribution (256 element long, 500 ensembles).

Particle Number	Disorder	Average Mass	5% Peak	10% Peak	70% Peak	90% Peak	Peak	Zero Crossing
130th particle	$\xi = 0.0$	1.0000	1.0462	1.0365	1.0002	0.9911	0.9808	0.9560
	$\xi = 0.1$	1.0000	1.0462	1.0365	1.0002	0.9911	0.9817	0.9560
	$\xi = 0.2$	1.0000	1.0508	1.0409	1.0032	0.9938	0.9839	0.9560
	$\xi = 0.35$	1.0000	1.0623	1.0515	1.0100	0.9994	0.9881	0.9525
	$\xi = 0.5$	1.0000	1.0735	1.0616	1.0155	1.0035	0.9906	0.9449
	$\xi = 0.8$	1.0000	1.0841	1.0713	1.0211	1.0079	0.9933	0.9328
150th particle	$\xi = 0.0$	1.0000	1.0402	1.0317	0.9990	0.9910	0.9825	0.9597
	$\xi = 0.1$	1.0000	1.0419	1.0332	1.0003	0.9920	0.9835	0.9599
	$\xi = 0.2$	1.0000	1.0464	1.0373	1.0032	0.9946	0.9855	0.9597
	$\xi = 0.35$	1.0000	1.0574	1.0475	1.0095	0.9998	0.9894	0.9566
	$\xi = 0.5$	1.0000	1.0678	1.0569	1.0146	1.0036	0.9917	0.9500
	$\xi = 0.8$	1.0000	1.0782	1.0664	1.0199	1.0076	0.9939	0.9387
200th particle	$\xi = 0.0$	1.0000	1.0330	1.0258	0.9991	0.9924	0.9856	0.9665
	$\xi = 0.1$	1.0000	1.0342	1.0271	1.0001	0.9933	0.9862	0.9666
	$\xi = 0.2$	1.0000	1.0376	1.0303	1.0023	0.9954	0.9878	0.9665
	$\xi = 0.35$	1.0000	1.0459	1.0380	1.0073	0.9995	0.9910	0.9642
	$\xi = 0.5$	1.0000	1.0537	1.0450	1.0113	1.0025	0.9929	0.9587
	$\xi = 0.8$	1.0000	1.0620	1.0526	1.0155	1.0056	0.9947	0.9494
220th particle	$\xi = 0.0$	1.0000	1.0308	1.0242	0.9992	0.9930	0.9864	0.9685
	$\xi = 0.1$	1.0000	1.0320	1.0253	1.0000	0.9937	0.9870	0.9686
	$\xi = 0.2$	1.0000	1.0350	1.0282	1.0020	0.9954	0.9884	0.9685
	$\xi = 0.35$	1.0000	1.0426	1.0352	1.0066	0.9993	0.9914	0.9665
	$\xi = 0.5$	1.0000	1.0500	1.0419	1.0105	1.0022	0.9933	0.9619
	$\xi = 0.8$	1.0000	1.0575	1.0487	1.0142	1.0050	0.9949	0.9542

Table 5. Unscaled Coherent Wave Velocity Picking ($\sqrt{\widetilde{M}_1}$) for different particles before and after localization length for a disordered chain with normal distribution (256 element long, 500 ensembles).

Particle Number	Disorder	Average Mass	5% Peak	10% Peak	70% Peak	90% Peak	Peak	Zero Crossing
130th particle	$\xi = 0.1$	1.0000	1.0462	1.0366	1.0002	0.9912	0.9818	0.9560
	$\xi = 0.2$	1.0000	1.0509	1.0409	1.0033	0.9939	0.9840	0.9560
	$\xi = 0.35$	1.0022	1.0614	1.0505	1.0091	0.9985	0.9872	0.9515
	$\xi = 0.5$	1.0274	1.0595	1.0477	1.0022	0.9904	0.9776	0.9322
	$\xi = 0.8$	1.1581	1.0081	0.9962	0.9496	0.9373	0.9237	0.8668
150th particle	$\xi = 0.1$	1.0000	1.0420	1.0332	1.0003	0.9921	0.9835	0.9599
	$\xi = 0.2$	1.0000	1.0465	1.0374	1.0032	0.9946	0.9856	0.9597
	$\xi = 0.35$	1.0022	1.0564	1.0465	1.0086	0.9989	0.9885	0.9556
	$\xi = 0.5$	1.0274	1.0539	1.0431	1.0013	0.9905	0.9787	0.9373
	$\xi = 0.8$	1.1581	1.0026	0.9917	0.9485	0.9370	0.9243	0.8723
200th particle	$\xi = 0.1$	1.0000	1.0343	1.0271	1.0001	0.9934	0.9862	0.9666
	$\xi = 0.2$	1.0000	1.0377	1.0304	1.0024	0.9954	0.9879	0.9665
	$\xi = 0.35$	1.0022	1.0449	1.0370	1.0064	0.9985	0.9901	0.9631
	$\xi = 0.5$	1.0274	1.0399	1.0313	0.9981	0.9894	0.9799	0.9458
	$\xi = 0.8$	1.1581	0.9876	0.9788	0.9443	0.9351	0.9250	0.8822
220th particle	$\xi = 0.1$	1.0000	1.0320	1.0253	1.0000	0.9937	0.9870	0.9686
	$\xi = 0.2$	1.0000	1.0320	1.0253	1.0000	0.9937	0.9870	0.9685
	$\xi = 0.35$	1.0022	1.0417	1.0343	1.0057	0.9984	0.9905	0.9654
	$\xi = 0.5$	1.0274	1.0362	1.0283	0.9972	0.9891	0.9803	0.9490
	$\xi = 0.8$	1.1581	0.9834	0.9752	0.9431	0.9346	0.9252	0.8867

Table 6. Coherent Wave Velocity calculated from the time taken by the pulse to travel a common distance of separation (7 particles/elements) with time calculated in reference to $5\%, 10\%, 70\%, 90\%$ of the peak value and the peak value of the coherent wave packet.

Particle Number	Disorder	5% Peak	10% Peak	70% Peak	90% Peak	Peak	Zero Crossing
	$\xi = 0.0$	1.0466	1.0321	0.9954	0.9867	0.9780	0.9571
	$\xi = 0.1$	1.0466	1.0369	0.9999	0.9910	0.9823	0.9613
27th particle -	$\xi = 0.2$	1.0515	1.0417	0.9999	0.9910	0.9823	0.9613
20th particle	$\xi = 0.35$	1.0665	1.0565	1.0089	0.9999	0.9910	0.9654
	$\xi = 0.5$	1.0820	1.0665	1.0135	0.9999	0.9910	0.9696
	$\xi = 0.8$	1.0925	1.0820	1.0227	1.0135	0.9999	0.9531
	$\xi = 0.0$	1.0135	1.0089	0.9999	0.9954	0.9954	0.9867
157th particle	$\xi = 0.1$	1.0107	1.0082	0.9982	0.9960	0.9930	0.9867
- 150th	$\xi = 0.2$	1.0105	1.0080	0.9974	0.9957	0.9928	0.9867
particle	$\xi = 0.35$	1.0072	1.0054	0.9984	0.9965	0.9948	0.9910
	$\xi = 0.5$	1.0056	1.0041	0.9983	0.9964	0.9940	0.9867
	$\xi = 0.8$	1.0106	1.0072	0.9947	0.9917	0.9880	0.9780
	$\xi = 0.0$	1.0135	1.0089	0.9999	0.9954	0.9954	0.9910
227th particle	$\xi = 0.1$	1.0090	1.0073	0.9969	0.9959	0.9948	0.9867
- 220th	$\xi = 0.2$	1.0074	1.0056	0.9968	0.9951	0.9934	0.9867
particle	$\xi = 0.35$	1.0056	1.0039	0.9957	0.9939	0.9917	0.9867
	$\xi = 0.5$	1.0059	1.0039	0.9968	0.9950	0.9926	0.9867
	$\xi = 0.8$	1.0122	1.0111	1.0062	1.0049	1.0031	0.9867
	$\xi = 0.0$	1.0089	1.0089	0.9999	0.9999	0.9954	0.9910
247th particle	$\xi = 0.1$	1.0087	1.0060	0.9975	0.9966	0.9953	0.9910
- 240th	$\xi = 0.2$	1.0073	1.0047	0.9964	0.9952	0.9925	0.9910
particle	$\xi = 0.35$	1.0041	1.0019	0.9946	0.9928	0.9909	0.9954
	$\xi = 0.5$	1.0017	1.0002	0.9928	0.9916	0.9903	$----$
	$\xi = 0.8$	0.9937	0.9919	0.9860	0.9846	0.9847	$----$